Interaction Potentials, Spectroscopy and Transport Properties of RG+/He (RG=Ar-Rn)

Timothy Wright, Larry Alan Viehland, Ben R Gray

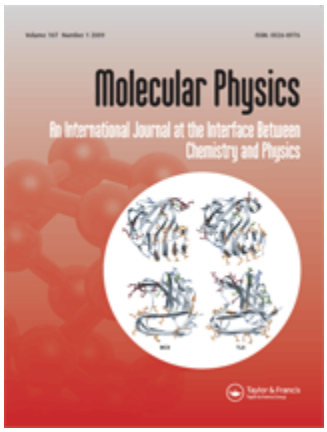

Interaction Potentials, Spectroscopy and Transport Properties of RG+/He (RG=Ar-Rn)

Journal:	*Molecular Physics*
Manuscript ID:	TMPH-2009-0172.R1
Manuscript Type:	Full Paper
Date Submitted by the Author:	06-Jul-2009
Complete List of Authors:	Wright, Timothy; University of Nottingham, School of Chemistry Viehland, Larry Gray, Ben; University ogf Nottingham
Keywords:	ionic complexes, ion mobility, spectroscopy

Interaction Potentials, Spectroscopy and Transport Properties of RG^+–He (RG=Ar–Rn)

Larry A. Viehland,
Department of Science,
Chatham University,
Pittsburgh, PA 15232, USA

Benjamin R. Gray and Timothy G. Wright,
School of Chemistry,
University of Nottingham, University Park,
Nottingham, NG7 2RD, UK

Abstract

High-level *ab initio* potential energy curves are calculated for the RG^+–He complexes (RG =Ar–Rn). RCCSD(T) calculations are employed with large basis sets, and taking account of spin-orbit coupling. The calculated spectroscopic parameters are compared to experimentally-determined values, to other high-level *ab initio* results, and to results from potentials that were obtained by fitting to experimental data. The gas-phase mobilities of RG^+ ions in He are calculated from our potentials and compared, graphically and statistically, to the experimental mobilities as a function of E/n_0 at several temperatures. We conclude that more precise experimental data are required in order to discriminate between potentials with more certainty. In addition, we discuss previously reported, unexpectedly large drops in experimental mobility values for RG^+ in He at 4.35 K as $E/n_0 \rightarrow 0$.

I. Introduction

Recently, we presented[1] high-quality *ab initio* potential energy curves for the Ne^+–He and He^+–Ne complexes, and compared calculated spectroscopic parameters and transport coefficients with those previously available and with new experimental mobility data. In general, the agreement was excellent, the only exception being the comparison with some of the experimental spectroscopic data[2] for Ne^+–He. In the present study, we extend our work to the heavier rare gas atomic cations interacting with He. As before, we aim to produce high quality *ab initio* curves, to employ these in the derivation of spectroscopic and transport quantities, and to compare them to available experimental values. Mobilities are useful in understanding chemical reactions, such as those in plasmas. In addition, they provide a good experimental test of calculated potentials, over a wider range of internuclear separations than is generally possible using spectroscopic or scattering techniques. The latter is particularly important for open-shell species, which are often difficult to generate experimentally, and additionally there are questions as to which potentials to be used, depending on the spin-orbit states present in the experiment, which can depend on the experimental conditions.[1] Reliable potentials, of course, are useful across a wide range of chemistry, but they are fo greater use if their reliability has been tested.

An early report of spectra by Tanaka *et al.*[3] was extended by Dabrowski, Herzberg and Yoshino (DHY),[4] who published a detailed UV absorption spectroscopic study of the Ar^+–He complex. Since the ground state of Ar^+ is ^2P, interaction with He gives $^2\Pi$ and $^2\Sigma^+$ electronic states in the absence of spin-orbit coupling, with the latter state expected to be lower in energy owing to less electron repulsion along the internuclear axis. Spin-orbit coupling leads to $^2P_{3/2}$ and $^2P_{1/2}$ states of Ar^+ which, upon interaction with He, yield $^2\Sigma_{1/2}{}^+$, $^2\Pi_{3/2}$ and $^2\Pi_{1/2}$ molecular states; the first two correlate with the lower, $^2P_{3/2}$ + He asymptote, and the third with the higher, $^2P_{1/2}$ + He one. The molecular states, according to a Hund's case (a) analysis, are thus $X^2\Sigma_{1/2}{}^+$, $A_1{}^2\Pi_{3/2}$ and $A_2{}^2\Pi_{1/2}$. Emission lines were observed by DHY, giving spectroscopic information on the $A_2{}^2\Pi_{1/2}$ and $X^2\Sigma_{1/2}{}^+$ states, as discussed below.

Saito *et al.*[5] have estimated an Ar^+–He binding energy of 37 meV (~300 cm^{-1}) from mobility measurements. Carrington and coworkers[6] have recorded microwave spectra of Ar^+–He at energies close to the dissociation asymptote. These transitions are in regions where the Born-Oppenheimer approximation was found to break down, and a detailed treatment of the energy levels was presented. The transitions observed in that work, together with those from DHY, were employed to generate fitted potential energy curves for all three states mentioned above; this set of potentials was designated MAL1.

In addition to this fitted potential, other theoretical results are available for Ar^+–He. Early work focused on charge exchange, mainly concerned with nascent He^+ ions in Ar.[7,8] In 1978, Olson and Liu[9] calculated CI curves for the $X^2\Sigma^+$ and $A^2\Pi$ states of Ar^+–He in the absence of spin-orbit coupling. In 1985, Hausamann and Morgner[10] made use of theoretical and experimental data available at the time and a model to obtain potential energy curves for Ar^+–He, Kr^+–He and Xe^+–He that included spin-orbit coupling. Soon afterwards, Siska[11] reported the results of a modified Tang-Toennies model for the potential energy curves for Ar^+–He, but in the absence of spin-orbit coupling. An MRDCI study by Stärk and Peyerimhoff[12] in 1986

considered a number of low-lying states of the $[Ar\text{-}He]^+$ system, with the lowest $^2\Sigma^+$ and $^2\Pi$ states corresponding to Ar^+–He; owing to emphasis being placed on the excited states, they did not achieve an optimal description of the lower states that are pertinent to the present study. Potential curves were also obtained by Brunetti *et al.*[13] by fitting an expression to the spectroscopic data and assuming the spin-orbit coupling was equal to that of the separated atoms and independent of the internuclear separation. Balasubramanian *et al.*[14] reported non-spin-orbit curves for Ar^+–He.[15] In 1990, Staemmler[16] reported ab initio calculations at the SCF and CEPA levels using large Gaussian basis sets for the lowest states of Ar^+–He; spin-orbit effects were added using a semi-empirical treatment. Gemein and Peyerimhoff[17] used MRD-CI calculations, both with and without spin-orbit coupling, to calculate potential energy curves, reporting equilibrium bond lengths, dissociation energies and harmonic vibrational frequencies. In 1991, Viehland, Viggiano and Mason (VVM)[18] combined the SCF and CI potentials of Olson and Liu[9] with the known long-range behaviour to obtain potentials (without spin-orbit effects) for the $^2\Sigma^+$ and $^2\Pi$ states of Ar^+–He; the Siska[11] potentials were also employed, but in a modified form. Ionization energies for RG–He and the associated spectroscopic parameters for RG^+–He have been reported by Ma, Li and Ng[19]; no spin-orbit coupling was included. In 2001, Murrell *et al.*[20] reported non-SO and SO potential energy curves for Ar^+–He over a limited range using MRCI+Q energies and an aug-cc-pVQZ basis set. Most recently, to our knowledge, Bera *et al.*[21] have reported UCCSD(T)/aug-cc-pVTZ spectroscopic and potential parameters for Ar^+–He. In the present work, we shall compare the above results with our potential energy curves, and additionally assess them against other experimental data.

The large body of data on Ar^+–He is not matched for the Kr^+–He ion. Early experimental work comprises the UV emission spectra from Tanaka *et al.*[3] where the assignment was only tentative, and scattering studies of He^+ and Kr by Weise.[22] The transport studies of Saito *et al.*[5] suggested that the binding energy of the Kr^+–He ground state was ~29 meV (~230 cm^{-1}). There are model potential results for Kr^+–He from Hausamann and Morgner[10] and relativistic CI calculations by Balasubramanian *et al.*[23], where spin-orbit coupling was included using basis sets of approximately double-ζ quality.[15] Ma *et al.*[19] also reported spectroscopic and potential parameters for Kr^+–He. The most detailed information, however has come from a joint microwave and theoretical study by Carrington and coworkers.[24] At present, the fitted (MAL1) interaction potential reported in that work (similar to that obtained for Ar^+–He, mentioned above) represents most of the information that is known for this species.

To our knowledge, there is no experimental or theoretical spectroscopic information available for Xe^+–He or Rn^+–He, except for the model potential calculations for Xe^+–He, by Hausamann and Morgner.[10]

Experimental studies have been performed on the transport of RG^+ ions through He. We have already mentioned our previous work on Ne^+ in He[1], but all of the other RG^+ ions (except Rn) have also been studied. The mobility of Ar^+ through He has been studied at a number of temperatures: at 4.35 K by Saito *et al.*[5]; at 82 K by Koizumi *et al.*[25]; at 92, 170, 293, 428 and 552 K by Viehland *et al.*;[18] and at 300 K by Lindinger and Albritton.[26] By calculating theoretical transport coefficients and comparing to the experimental data, it is possible to test the potential (or conversely the experimental

data) over a wide range of internuclear separations.[27] Generally, such tests are more stringent than comparison with spectroscopic data, as the latter usually only sample a very small region of internuclear separation. One of the present species is an exception, however, since spectroscopic data close to the minimum,[4] as well as at very long range[6] are available for Ar^+–He.

For Kr^+ in He, the mobilities having been measured at: 4.35 K by Saito *et al.*[5]; 82 K by Koizumi *et al.*[28]; 294 K by Jones *et al.*[29]; and 300 K by two groups, Johnsen *et al.*[30] and Kaneko *et al.*[31] For Xe^+ in He, only two sets of data have been reported: at 82 K by Koizumi *et al.*[28], and at 295 K by Johnsen *et al.*[30]

II. Calculations

A. *Ab initio Potentials*

The calculations reported here were performed at the RCCSD(T) level of theory, employing d-aug-cc-pV5Z quality basis sets for He–Ar; the frozen core approximation was used throughout. The basis sets were doubly-augmented to allow a good description of the long-range interactions, with the double-diffuse augmentation being achieved by extending the basis set by one set of functions of each angular momentum type; the ζ values were obtained by even-tempered extrapolations of the two most diffuse functions of the same type in the standard basis set. For the heavier atoms, small-core relativistic effective core potentials (ECPs) were employed: ECP10MDF, ECP28MDF and ECP60MDF for Kr, Xe and Rn, respectively; the standard aug-cc-pV5Z valence basis sets[32] were then used with these ECPs, again extending the basis set by one diffuse function of each type, as described above. The potential energy curves of the $^2\Sigma^+$ and $^2\Pi$ electronic states were calculated point by point using the MOLPRO[33] suite of programs. A full counterpoise correction was made at each point to correct for basis set superposition error.

Since the interaction between He and RG^+ is expected to be weak, the spin-orbit coupling is expected to be localized on Ar^+, as was assumed in ref. 6. We therefore derived the SO potentials analytically, using expressions arising from the well-known atomic model[34] that connects the SO-potentials, $X^2\Sigma_{1/2}{}^+$, $A_1{}^2\Pi_{3/2}$ and $A_2{}^2\Pi_{1/2}$ (denoted V_X, V_{A_1} and V_{A_2}), to the $^2\Sigma^+$ and $^2\Pi$ potentials (denoted V_Σ and V_Π). These expressions are

$$V_X = \frac{1}{2}(V_\Sigma + V_\Pi + \Delta - \delta) \quad (1)$$

$$V_{A_1} = V_\Pi \quad (2)$$

and

$$V_{A_2} = \frac{1}{2}(V_\Sigma + V_\Pi + \Delta + \delta), \quad (3)$$

where

$$\delta^2 = (V_\Sigma - V_\Pi)^2 - \frac{2\Delta}{3}(V_\Sigma - V_\Pi) + \Delta^2 \quad (4)$$

and Δ is the SO splitting between the RG^+ atomic $^2P_{3/2}$ and $^2P_{1/2}$ states. The values of Δ are 1431.41, 5371.0, 10537.01 and 30895.1 cm^{-1} for RG = Ar–Rn, respectively.[35]

B. Spectroscopic Constants

Once obtained, the potential energy data set was used as input into the LEVEL program[36] in order to obtain spectroscopic and other data, in particular the rovibrational energy levels. From the latter, fits of the lowest few levels to standard spectroscopic formulae were employed to obtain equilibrium values.

C. Transport Properties

To obtain transport coefficients, the calculated potentials were first employed in the QVALUES program[37,38] to obtain transport cross sections with a precision of 0.1%. Transport coefficients were obtained by employing these cross sections in the GC program,[39] a modified version of the older GRAMCHAR program.[40] The modifications were made to cope with the increased demands when the ion mobility has both a maximum and a minimum (as was the case for systems involving the coinage metal cations moving through the rare gases[39]), to allow higher-order approximations to be employed, and finally to take advantage of faster, modern computers.

The overall precision for the calculated mobilities is 0.1% at small E/n_0 (the ratio of the electric field strength to the gas number density). In the worst cases, it is 1% near and beyond the mobility maximum, but only 3% in the region between the minima and maximum, where the mobility is increasing rapidly with increasing E/n_0.

Calculated values for the mobilities and other transport coefficients for each one of the naturally-occurring RG^+ isotopes in He have been obtained over wide ranges of E/n_0 at gas temperatures of 100, 200, 300, 400 and 500 K, and for gas temperatures that have been used in transport experiments (see above). All of these results have been entered into the database maintained at Chatham University.[41]

III. Results and Discussion

A. Potential Curves and Spectroscopy

In Figure 1, we show our *ab initio* calculated potential energy curves for Ar^+–He, along with the MAL1 potentials[6]. As may be seen, the two sets of curves are in very good agreement, and although there are differences at the minima, the directions of these differences are not consistent for the three SO states. (The data points for our curves are given as Supplementary Material.)

We start by commenting on the *ab initio* results that did not include SO coupling, although such studies cannot be assessed against experimental data directly. Results prior to the work in ref. 6 have been commented on previously[6,24]. The more recent work of Murrell *et al*.[20] reports the results of MRCI+Q calculations employing an

aug-cc-pVQZ basis set. We have noted previously[1] that for Ne^+–He a single-reference method appears to be satisfactory and we assume the same is true for the species considered herein. For Ar^+–He, this certainly seems to the case since the derived R_e and D_e values in Table 1 for the MRCI[20] and the present RCCSD(T) potentials are very close, both for the $^2\Sigma^+$ and the $^2\Pi$ states. The most recent study by Bera *et al*.[21] reports CCSD(T) calculations employing aug-cc-pVTZ basis sets for the $^2\Sigma^+$ state. Since the Gaussian program[42] was employed therein, we assume that unrestricted wave functions were used. A number of calculations were employed, including the DFT hybrid method, B3LYP, as well as MP2 and CCSD(T). The B3LYP values indicated a large overestimate of the interaction, something that has been noted previously by one of us for NO^+–Ar.[43] The MP2 and CCSD(T) results[21] are much closer to each other, with the CCSD(T) values being closer to the results of the present study (see Table 1). We note that results were also reported where all electrons were correlated, at both the MP2 and CCSD(T) levels; however, since no tight functions were included to describe the core-valence correlation, those results must be viewed with caution. We only include the frozen core CCSD(T) results in Table 1, for which good agreement is seen for R_e, but the well depths are shallower than those found herein.

Moving on to studies which have included SO coupling, we only consider the most recent and reliable potentials, the key aspects of which are presented in Table 2. (The other potentials are commented upon in refs. 6 and 18.) We first note that the model potential results of Siska[11] and a modified version of these[18] were mainly fitted to the UV results of Dabrowski *et al*.[4], whereas the MAL1 potentials also have input from the microwave spectrum that helps characterize the long-range region better. As noted before, [6] there are significant differences between the three aforementioned potentials, with the differences being largest for the A_1 state, for which there were no observed transitions in the UV study. Comparing these to the present results and to the MAL1 potential, we see that the present R_e value is slightly larger, with the D_e value being slightly smaller; interestingly the present value falls between the previously determined values. For the A_2 state, we obtain excellent agreement with the D_e value from the MAL1 potential,[6] and indeed with the value from Siska.[11] All of these values lie significantly above those of VVM[18] and the value from DHY.[4] In the latter case, dissociation energies were obtained from a combination of extrapolation and energy differences, so perhaps it is not surprising that the value is not so accurate. Lastly, the most dramatic differences in D_e values occur for the A_1 state, for which there were no experimental data; however, since the three states here are interconnected *via* spin-orbit coupling, knowing two of them defines the third. It may be seen from Table 2 that the present work is in excellent agreement with the MAL1 potentials for both R_e and D_e. In conclusion, the MAL1 potentials, having included long-range spectroscopic data in the fit, appear to be much more reliable potentials than either of the two earlier ones, which were based purely on the UV spectra. The MAL1 potentials are in very good agreement with the curves obtained in the present work. We note that there is also very good agreement with the SO results reported in ref. 20 for the X and A_2 states (no parameters were reported for the A_1 state).

For Kr^+–He, there is no assigned UV spectrum. Hence, all of the information on this species comes from the microwave study of Carrington and coworkers[24] on levels that are only a few cm^{-1} from the dissociation limit. Thus, these experiments sample only

the long-range portion of the interaction potential. Since microwave spectroscopy is such a precise technique, the whole potential curve should be obtainable, in principle, if enough transitions are observed. In fact, sufficient transitions were observed[24] to generate MAL1 potentials, similar in type to those for Ar^+–He, but now having no input from UV spectra. These MAL1 potential are, therefore, *only* defined in terms of transitions between levels very close to the dissociation limits.

As may be seen in Figure 2, the agreement between our Kr^+–He potentials and the MAL1 potentials looks very good, with the MAL1 potentials being very slightly deeper in all cases, especially for the *X* state. These features are evident in the data presented in Table 2. Given that the MAL1 potentials have been obtained by fitting only to transitions between high-lying levels, the agreement between the two sets of curves is remarkable.

We note in passing that the previous study by Balasubramanian *et al.*[15] has been noted as having an error[24], as the ground state is designated $X^2\Pi_{3/2}$, and the dissociation energies are far from those obtained here or from the MAL1 potentials. However, the estimate for the binding energy of 29 meV (~230 cm^{-1}) from mobility studies[5] is of the correct magnitude.

There are no reliable data to which to compare our results for either Xe^+–He or Rn^+–He, although in the former case there are experimental mobility results, and these will be considered below.

B. Transport Results for Ar^+ in He

As noted in the Introduction, there have been a number of studies measuring the mobility of Ar^+ in He at a variety of temperatures. Such studies can, if there are enough data points, and if the accuracy and precision are high enough, provide stringent tests of potentials across a very wide range of internuclear separation.[27] To this end, we have calculated mobilities using both the MAL1 and the present potentials, and have compared the results to experimental data. In Figure 3, the results at 300 K are given, both those calculated from the present potentials and the experimental data points.

For the calculations, we have employed a (110) weighting of the cross sections arising from the *X*, A_1 and A_2 potentials, which is akin to assuming only the $^2P_{3/2}$ atomic state of Ar^+ is present. We have also used a (001) weighing, which is for the $^2P_{1/2}$ state. We have performed such calculations for both the MAL1 and present potentials. Unfortunately, the cited experimental error bars are large enough that they encompass both of the calculated curves. If it is assumed that the error bars are pessimistic, then by eye it appears that the (110) weighting of the potentials is in better agreement with the actual experimental data points than the (001) one. In agreement with our conclusion for Ne^+ in He[1], this would suggest that only the $^2P_{3/2}$ ground state of Ar^+ were present in the experiments, i.e., any ions created in the higher SO state were efficiently quenched to the lower state before they reached the drift region of the apparatus.

Another way of comparing data is to employ the statistical quantities δ and χ.[38] The dimensionless quantity δ is a measure of the relative differences compared to the combined experimental and calculational errors, while χ is a measure of the relative standard deviation to the sum of the squared error estimates. Values of $|\delta|$ that are substantially lower (alternatively, higher) than 1 indicate that there is substantial agreement (disagreement) between the calculated and measured values, on average. Values of χ that are not much larger than $|\delta|$ indicate that there is little scatter in the experimental data and that the agreement between the calculated and measured values is uniform over all values of E/n_0, while values of χ substantially greater than $|\delta|$ indicate that at least one of these factors is not true. In Table 3, we report these quantities for the present potential and smoothed versions[44,45,46] of the experimental data for $^{40}Ar^+$ in He, but not including the experimental values for $E/n_0 < 2$ Td (see below). What is immediately clear is that for the data at the higher temperatures (≥293 K) there is agreement between calculated and experimental data for either state, which is a result of the large experimental error bars, as can be seen in Figure 3. These statistical quantities also indicate that, with regards to the mobility data, there is no statistical difference between the results obtained using the present potentials and those obtained using the MAL1 potentials.

The mobility data from VVM[23] for RG^+ in He have been suspected[47,48] for many years of being less accurate than claimed by the experimenters. Hence it is not surprising to find in Table 3 that these data are in significant disagreement with the present calculations, as they are in similar disagreement with results calculated from all of the other available potentials.

The data which have the smallest error bars are those at 4.35 K.[5] Interestingly, the experimental data show a distinct drop in the mobility of RG^+ in He as $E/n_0 \rightarrow 0$ — see Figure 4. Similar results had been reported previously for He^+ in He,[49] a system in which resonant charge transfer (RCT) occurs. One explanation that has been put forward[5] is quantum effects, as previously predicted by Dickinson[50] and Heiche and Mason.[51] The same unusual mobility behaviour was found in N_2^+ and CO^+ in He by Sanderson *et al.*[52] in which RCT cannot occur, and in this case orbiting resonances and/or collision-induced rotational excitation were proposed. Other experiments have also observed such unusual low-E/n_0 mobilities, in He for Ne^+,[5,53] O_2^+,[54] NO^+,[55] and other ions.[56] A first theoretical account of the low E/n_0 anomalous mobilities of N_2^+ and O_2^+ in He at 4.35 K was presented by Ohtsuki *et al.*[57] They calculated mobilities from MRCI potentials, and demonstrated that the anomalous behavior was due to Feshbach-like resonances, where rotational excitation of the molecular ions occurred as a result of collisions with He. This explanation cannot apply to atomic ions such as RG^+ in He, of course, nor for other atomic ions, O^+ and N^+,[58] for which similar behaviour has been found. The suggestion that quantum effects might be the source of the low E/n_0 behaviour was tested explicitly by Viehland and Hurly in 1996[48] and was found not to explain the observed results. As such, the anomalous low E/n_0 behaviour of atomic ions in He at 4.35 K so far remains unexplained.

The fact that the present results, as was the case for Ne^+ in He,[1] also show that the theoretical mobilities do not show the dramatic fall in values as $E/n_0 \rightarrow 0$ has led us to consider this issue further. We note that, in ref. 5, the ions were provided with a constant injection energy of 20 eV. Consequently, the value of E/n_0 is controlled by varying the pressure, and hence low E/n_0 values are achieved at higher pressures. At

4.35 K, there is a possibility for He_2 (and possibly higher-order clusters) to form, and since the formation would be a termolecular process (with a third body being required to stabilize the He_2 species) it would be highly pressure dependent. The effect of He dimer formation would be to increase the effective reduced mass of collisions, and hence lower the mobility. This hypothesis could be tested by performing measurements at E/n_0 values where both E and the pressure were changed, but yielding the same resulting E/n_0 value.

B. Other Transport Results

Figures 5 and 6 compare calculated and experimental mobilities for $^{84}Kr^+$ in He at 300 and 4.35 K, respectively. In Table 4, we report the statistical quantities from a comparison of the present potential for $^{84}Kr^+$ in He and smoothed versions[40,41,44] of the experimental data in which neither the isotope nor the state was specified. The calculated mobilities for the five naturally occurring isotopes of Kr are very similar. This is consistent with the theoretical prediction (from the first approximation of the two-temperature kinetic theory[59]) that the mobility is inversely proportional to the square root of the reduced mass. Hence any differences between theory and experiment shown in Table 4 are not due to which isotope was used.

Again we note that calculated mobilities involving the MAL1 potentials are not statistically different from those using the present potentials — more evidence for their close agreement. Table 4 shows that at 4.35 K there is agreement between calculated and experimental data for either state. Note that again we do not include the experimental values for $E/n_0 < 2$ Td at 4.35 K, for the reasons we have discussed for Ar^+ in He above. The data at 82 K are in satisfactory agreement with the calculations for both states, owing to our use of 4% as the experimental accuracy; the experimenters did not state the accuracy of their results, but examination of the raw data[28] shows rapid variations by as much as 4%. Finally, the data near room temperature are in good to excellent agreement with the calculations for the $^2P_{1/2}$ excited state but not with those for the $^2P_{3/2}$ ground state.

As shown in Figures 4 and 6, a small mobility minimum occurs at low gas temperatures. Such minima arise frequently with open-shell ions, because the R^{-6} component of their long-range interactions with rare gas atoms is large, compared to the R^{-4} component that dominates at the very largest separations. More extensive comments about mobility minimum have been given previously.[39]

The calculated mobilities for $^{132}Xe^+$ in He at 300 K are compared with experimental values in Figure 7 and Table 5. As before, the calculated mobilities for different isotopes are very similar, so difference between theory and experiment are not due to which isotope was used. The data at 82 K are in reasonable agreement with the calculations for both states, owing to our choice again to use 4% for the accuracy, a value that was not reported by the experimenters.[28] The data near room temperature are not in good agreement with the calculations, suggesting that those data may be even less accurate than the estimate of 5% made by the experimenters[27].

There are no experimental values for Rn^+ in He, and so the quantities calculated here and placed into the database[41] represent the only values available.

A word of caution is in order, however, as we previously[1,60] noted problems arising from injection effects when a heavy ion is passed into a drift tube containing a light gas; this can lead to a measured mobility that is too high and careful checking of experimental values is required.

IV. Conclusions

The favourable comparison of the present, completely *ab initio*, potentials with previous experimental (DHY[4]) results and fitted MAL1[6,24] results for Ar^+–He and Kr^+–He, suggests that the present results are reliable. It is noteworthy that, for the most part, there is agreement with the MAL1 potentials of Carrington *et al.*[6,24] and the non-SO potentials of Siska[11] and VVM.[18] The discrepancies between those results and ours are likely in part attributable to different parameterizations and the different experimental data sets employed. The good agreement with the Kr^+–He MAL1 potentials[24] is particularly noteworthy, since the latter was obtained by fitting only to experimental spectroscopic data obtained from transitions between levels within a few cm^{-1} of the dissociation limit.

The agreement in Table 2 of our calculated spectroscopic quantities with those obtained from UV absorption spectra[4] is good, in the main. However, independent checking of some values is desirable, particularly for the dissociation energies.

Transport coefficients are known to be good tests of interaction potentials across a very wide range of interatomic (or intermolecular) separation, but such tests are reliant on the experimental precision being sufficiently good. The results above have shown that, near room temperature, the experimental errors of 5–7% are too large to be discriminatory for Ar^+ in He. We noted, however, that there appears to be a better agreement between the reported data points and the values calculated by assuming only Ar^+ ($^2P_{3/2}$) was present—a conclusion that would be consistent with our previous findings for Ne^+ in He[1], but somewhat contrary to comments made previously[5] regarding populations of the spin-orbit states. We have also noted that the distinct fall in the mobility values as $E/n_0 \rightarrow 0$ at 4.35 K is not in agreement with the theoretical predictions; this has been discussed previously,[48] where quantum chemical effects were ruled out. Since constant injection energies were employed in the mobility measurements and the low E/n_0 values were determined by increases in the pressure, we have conjectured that the presence of dimers (and other clusters) at 4.35 K could be the cause of the anomalous experimental results. We have suggested that these results should be independently checked in experiments where both E and n_0 are varied.

Finally, we note that the comments above regarding Ar^+–He and Kr^+–He suggest that the Xe^+–He and Rn^+–He potentials should also be reliable. In these cases, however, higher precision experimental results are required in order to test our potentials more definitively.

Acknowledgements

The work of L. A.V. was supported by the National Science Foundation under Grant CHE-0718024. T. G. W. is grateful to the EPSRC for the provision of computing time under the auspices of the NSCCS. B.R.G thanks the EPSRC and University of

Nottingham for an EPSRC DTA studentship. Dr. Mark Law (Aberdeen) and Prof. Jeremy Hutson (Durham) are thanked for providing the MAL1 potentials.

Table 1: Spectroscopic Parameters for He–RG^+ — Non-Spin-Orbit Curves. Isotopes employed are: ^{4}He, ^{40}Ar, ^{84}Kr, ^{131}Xe and ^{222}Rn. Here, the symbols represent the usual spectroscopic quantities: R_e is the equlibrium bond length, D_e is the depth of the potential;, D_0 is the energy between the zero-point and the asymptote, ω_e is the harmonic vibrational frequency, $\omega_e x_e$ is the anharmonicity constant, B_0 is the equilibrium rotational constant of the v = 0 level, D_{0J} is the first distortion constant for the v = 0 level, σ is the crossing point of the potential, when the potential = 0, and $\Delta G_{1/2}$ and $\Delta G_{3/2}$ are the first two vibrational term values.

System	State [Ref]	σ/ Å	R_e/ Å	D_e/ cm^{-1}	D_0/ cm^{-1}	ω_e/ cm^{-1}	$\omega_e x_e$/ cm^{-1}	B_0/ cm^{-1}	D_{0J}/ 10^{-5} cm^{-1}	$\Delta G_{1/2}$/ cm^{-1}	$\Delta G_{3/2}$/ cm^{-1}
He–Ar^+ $^2\Sigma^+$	This Work	2.05	2.41	420.1	341.2	164.3	17.31	0.754	8.33	130.2	94.1
	BBD[21] [a]		2.45	331		155.7	32.44		7.50	97.86	50.30
	GP[17]		2.47	274		186					
	MNG[20]		2.42	403							
$^2\Pi$	This Work	2.52	3.00	142.0	102.0	75.6	10.79	0.468	9.22	55.6	29.3
	GP[17]		3.12	113		140					
	MNG[20]		3.02	137							
He–Kr^+ $^2\Sigma^+$	This Work	2.30	2.68	301.7	240.0	127.9	14.57	0.578	6.28	99.4	68.4
$^2\Pi$	This Work	2.82	3.22	115.6	81.8	63.2	9.23	0.387	7.42	46.2	23.3
He–Xe^+ $^2\Sigma^+$	This Work	2.63	3.03	203.6	156.9	95.6	11.97	0.441	5.07	72.4	46.1
$^2\Pi$	This Work	3.11	3.52	87.8	60.2	58.0	9.31	0.316	5.87	39.4	20.8
He–Rn^+ $^2\Sigma^+$	This Work	2.73	3.15	184.0	141.0	87.7	11.15	0.406	4.71	66.2	41.6
$^2\Pi$	This Work	3.22	3.65	79.2	53.9	44.8	6.71	0.291	5.93	32.9	14.8

[a] CCSD(T)/FC values only cited from that work.

Table 2: Spectroscopic Parameters for He–RG^+ —Spin-Orbit Curves. Isotopes employed are: ^{4}He, ^{40}Ar, ^{84}Kr, ^{131}Xe and ^{222}Rn. Quantities are defined in Table 1.

System	Ref	σ/ Å	R_e/ Å	D_e/ cm^{-1}	D_0/ cm^{-1}	ω_e/ cm^{-1}	$\omega_e x_e$/ cm^{-1}	B_0/ cm^{-1}	D_0,/ 10^{-5} cm^{-1}	$\Delta G_{1/2}$/ cm^{-1}	$\Delta G_{3/2}$/ cm^{-1}
He–Ar$^+$ $^2\Sigma_{1/2}^+$	This work	2.18	2.60	271.1	215.5	117.6	13.60	0.643	10.4	90.9	62.3
	DHY[4]		2.585	262		120.3	13.60	0.659			
	Sis[11]	2.19	2.564	282.6							
	Sta[16]		2.66	242	190	116.9	17.7			83.9	55.2
	GP[17]		2.77	177		105					
	MNG[20]		2.62	258							
	MAL1[6]		2.573	281.6				0.651		93.2	64.1
	HM[10]	2.17	2.65	269.4	215.3						
$^2\Pi_{3/2}$	This Work	2.52	3.00	142.0	102.0	75.6	10.79	0.468	9.22	55.6	29.3
	Sta[16]		3.03	133	94	89.3	21.2			52.9	26.9
	GP[17]		3.10	105		80					
	MAL1[6]		2.98	143.4							
	HM[10]	2.59	2.96	161.3	114.5						
$^2\Pi_{1/2}$	This Work	2.52	2.88	178.1	131.7	91.6	12.58	0.512	8.33	68.0	38.2
	Sta[16]		2.91	166	121	102.2	21.7			64.0	35.1
	GP[17]		3.00	137		93					
	MNG[20]		2.89	169							
	DHY[4]		2.872	154				0.5146		69.2	
	Sis[11]	2.48	2.872	185.4							
	MAL1[6]		2.863	181.6				0.5160		68.9	
	HM[10]	2.51	2.86	192.8	140.3						

$He–Kr^+$ $^2\Sigma_{1/2}^+$	This Work	2.51	2.90	199.8	152.4	96.0	12.33	0.487	6.75	72.3	44.7
	HM[10]	2.51	2.91	240.4	183.1						
	MAL1[6]		2.87	208							
$^2\Pi_{3/2}$	This Work	2.82	3.22	115.6	81.8	63.2	9.23	0.387	7.42	46.2	23.3
	HM[10]	2.78	3.18	161.3							
	MAL1[6]		3.20	116							
$^2\Pi_{1/2}$	This Work	2.70	3.09	145.9	106.4	76.4	10.68	0.424	6.87	56.4	30.9
	HM[10]	2.65	3.04	192.8	140.3						
	MAL1[6]		3.06	149							
$He–Xe^+$ $^2\Sigma_{1/2}^+$	This Work	2.83	3.24	143.5	106.0	75.8	10.59	0.383	5.45	55.1	32.5
	HM[10]	2.25	2.65	403.3	327.5						
$^2\Pi_{3/2}$	This Work	3.11	3.52	87.8	60.1	58.0	9.31	0.316	5.87	39.4	20.8
	HM[10]	2.78	3.18	149.2	104.9						
$^2\Pi_{1/2}$	This Work	2.98	3.40	109.3	77.5	62.6	9.38	0.343	5.71	45.1	22.7
	HM[10]	2.59	2.59	22.6	167.8						
$He–Rn^+$ $^2\Sigma_{1/2}^+$	This Work	2.93	3.35	129.2	94.7	67.9	9.46	0.352	5.08	50.0	27.9
$^2\Pi_{3/2}$	This Work	3.22	3.65	79.2	53.9	44.8	6.71	0.291	5.93	32.9	14.8
$^2\Pi_{1/2}$	This Work	3.09	3.52	98.6	69.5	55.0	8.11	0.316	5.45	40.0	19.9

Table 3: Statistical Comparison between Calculated and Experimental Mobility Data for Ar^+ in He. See text for definitions of δ and χ. *N* is the number of data points, and %Expt and %Calc are the experimental and calculational precisions. When *N* is small, over-interpretation of the results should be avoided.

T/K	Data Source	State	E/n_0 Td	*N*	%Expt	%Calc	δ	χ
4.35	Ref. 39	$^2P_{3/2}$	2.0–11.5	7	2.0	0.1	0.25	0.34
			115–35.5	6	2.0	0.1	-1.23	1.39
		$^2P_{1/2}$	2.0–11.4	7	2.0	0.1	-0.16	0.22
			12.4–50.0	6	2.0	1.0	-0.79	1.33
82	Ref. 40	$^2P_{3/2}$	5.0–32.0	5	4.0	0.1	1.45	1.47
			32.0–70.0	4	4.0	0.5	0.79	1.05
		$^2P_{1/2}$	5.0–32.0	5	4.0	0.1	1.58	1.70
			32.0–70.0	4	4.0	0.5	2.30	2.38
92	Ref. 39	$^2P_{3/2}$	1.0–15.0	10	5.0	0.1	1.73	1.75
		$^2P_{1/2}$	1.0–15.0	10	5.0	0.1	1.62	1.65
170	Ref. 39	$^2P_{3/2}$	4.0–30.0	10	5.0	0.1	1.09	1.10
		$^2P_{1/2}$	4.0–30.0	10	5.0	0.1	1.29	1.35
293	Ref. 39	$^2P_{3/2}$	6.0–40.0	10	5.0	0.1	-0.62	0.62
		$^2P_{1/2}$	6.0–40.0	10	5.0	0.1	0.14	0.33
300	Ref. 41	$^2P_{3/2}$	5.0–50.0	10	7.0	0.1	-0.03	0.11
			50.0–130.0	8	7.0	0.1	-0.57	0.62
		$^2P_{1/2}$	5.0–50.0	10	7.0	0.1	0.67	0.70
			50.0–130.0	8	7.0	0.5	0.58	0.61
428	Ref. 39	$^2P_{3/2}$	8.0–50.0	10	5.0	0.1	-0.64	0.72
		$^2P_{1/2}$	8.0–50.0	10	5.0	0.1	0.48	0.75
552	Ref. 39	$^2P_{3/2}$	10.0–50.0	9	5.0	0.1	-0.46	0.53
		$^2P_{1/2}$	10.0–50.0	9	5.0	0.1	0.88	0.97

Table 4: Statistical Comparison between Calculated and Experimental Mobility Data for $^{84}Kr^{+}$ in He. See text for definitions of δ and χ. *N* is the number of data points, and %Expt and %Calc are the experimental and calculational precisions. When *N* is small, over-interpretation of the results should be avoided.

T/K	Data Source	State	E/n_0 Td	N	%Expt	%Calc	δ	χ
4.35	Ref. 39	$^2P_{3/2}$	2.0–11.5	7	2.0	0.1	0.07	0.19
			11.5–35.5	8	2.0	0.1	-0.34	0.54
		$^2P_{1/2}$	2.0–11.5	7	2.0	0.1	0.23	0.28
			11.5–50.0	6	2.0	0.3	-0.27	0.63
82	Ref. 39	$^2P_{3/2}$	4.0–32.0	10	4.0	0.1	0.64	0.65
			32.0–70.0	4	4.0	0.1	0.46	0.47
		$^2P_{1/2}$	4.0–32.0	10	4.0	0.1	0.54	0.57
			32.0–70.0	4	4.0	0.1	0.82	0.82
294	Ref. 40	$^2P_{3/2}$	3.0–45.0	5	4.0	0.1	-0.79	0.87
			45.0-250.0	5	4.0	0.1	-0.89	0.91
		$^2P_{1/2}$	3.0–45.0	5	4.0	0.1	-0.66	0.71
			45.0-250.0	5	4.0	0.1	0.02	0.53
300	Ref. 41	$^2P_{3/2}$	5.0–35.0	9	7.0	0.1	-1.87	1.93
			35.0–100.0	5	7.0	0.1	-1.73	1.87
		$^2P_{1/2}$	5.0–35.0	9	7.0	0.1	-0.49	0.53
			35.0–100.0	5	7.0	0.1	-0.09	0.25

Table 5: Statistical Comparison between Calculated and Experimental Mobility Data for $^{132}Xe^{+}$ in He. See text for definitions of δ and χ. *N* is the number of data points, and %Expt and %Calc are the experimental and calculational precisions. When *N* is small, over-interpretation of the results should be avoided.

T/K	Data Source	State	E/n_0 Td	N	%Expt	%Calc	δ	χ
82	Ref. 39	$^2P_{3/2}$	17.0–32.0	3	4.0	0.1	0.55	0.56
			32.0–70.0	5	4.0	0.1	0.20	0.43
		$^2P_{1/2}$	17.0–32.0	3	4.0	0.1	0.41	0.44
			32.0–70.0	4	4.0	0.1	0.33	0.46
295	Ref. 55	$^2P_{3/2}$	3.0–32.0	11	5.0	0.1	-1.24	1.28
			32.0-80.0	4	5.0	0.1	0.54	1.04
		$^2P_{1/2}$	3.0–32.0	11	5.0	0.1	-1.24	1.30
			32.0-80.0	4	5.0	0.1	-0.72	1.27

Figure Captions

Figure 1

Calculated potential energy curves for Ar^+–He. The solid black curves represent the present potential, calculated at the RCCSD(T)/d-aug-cc-pV5Z level of theory, while the red dashed ones represent the MAL1 potentials from ref. 6.

Figure 2

Calculated interaction energy curves for Kr^+–He. The black curves are the present ones, calculated at the RCCSD(T)/d-aug-cc-pV5Z level of theory — see text for details. The red dashed ones are the MAL1 potentials from ref. 24.

Figure 3

Standard mobilities for Ar^+ in He at 300 K. The points, with error bars are the experimental (smoothed) data points from refs. 44, 45, 46. The solid line is the calculated mobility curve assuming the $^2P_{3/2}$ state only is present; the dashed line is the calculated mobility curve assuming the $^2P_{1/2}$ state only is present. The ordinate is the standard mobility in $cm^2\ V^{-1}\ s^{-1}$, and the abscissa is the ratio of the electric field to the number density, in units of Townsend (Td).

Figure 4

Standard mobilities for Ar^+ in He at 4.35 K. The points, with error bars are the experimental data points from ref. 5. The solid line is the calculated mobility curve assuming the $^2P_{3/2}$ state only is present; the dashed line is the calculated mobility curve assuming the $^2P_{1/2}$ state only is present. The ordinate is the standard mobility in $cm^2\ V^{-1}\ s^{-1}$, and the abscissa is the ratio of the electric field to the number density, in units of Townsend (Td).

Figure 5

Standard mobilities for Kr^+ in He at 300 K. The points, with error bars are the experimental (smoothed) data points from refs. 44, 45, 46. The solid line is the calculated mobility curve assuming the $^2P_{3/2}$ state only is present; the dashed line is the calculated mobility curve assuming the $^2P_{1/2}$ state only is present. The ordinate is the standard mobility in $cm^2\ V^{-1}\ s^{-1}$, and the abscissa is the ratio of the electric field to the number density, in units of Townsend (Td).

Figure 6

Standard mobilities for Kr^+ in He at 4.35 K. The points, with error bars are the experimental data points from ref. 5. The solid line is the calculated mobility curve assuming the $^2P_{3/2}$ state only is present; the dashed line is the calculated mobility curve assuming the $^2P_{1/2}$ state only is present. The ordinate is the standard mobility in

$cm^2\ V^{-1}\ s^{-1}$, and the abscissa is the ratio of the electric field to the number density, in units of townsend (Td).

Figure 7

Standard mobilities for Xe^+ in He at 300 K. The points, with error bars are the experimental (smoothed) data points from refs. 44, 45, 46. The solid line is the calculated mobility curve assuming the $^2P_{3/2}$ state only is present; the dashed line is the calculated mobility curve assuming the $^2P_{1/2}$ state only is present. The ordinate is the standard mobility in $cm^2\ V^{-1}\ s^{-1}$, and the abscissa is the ratio of the electric field to the number density, in units of townsend (Td).

Figure 1

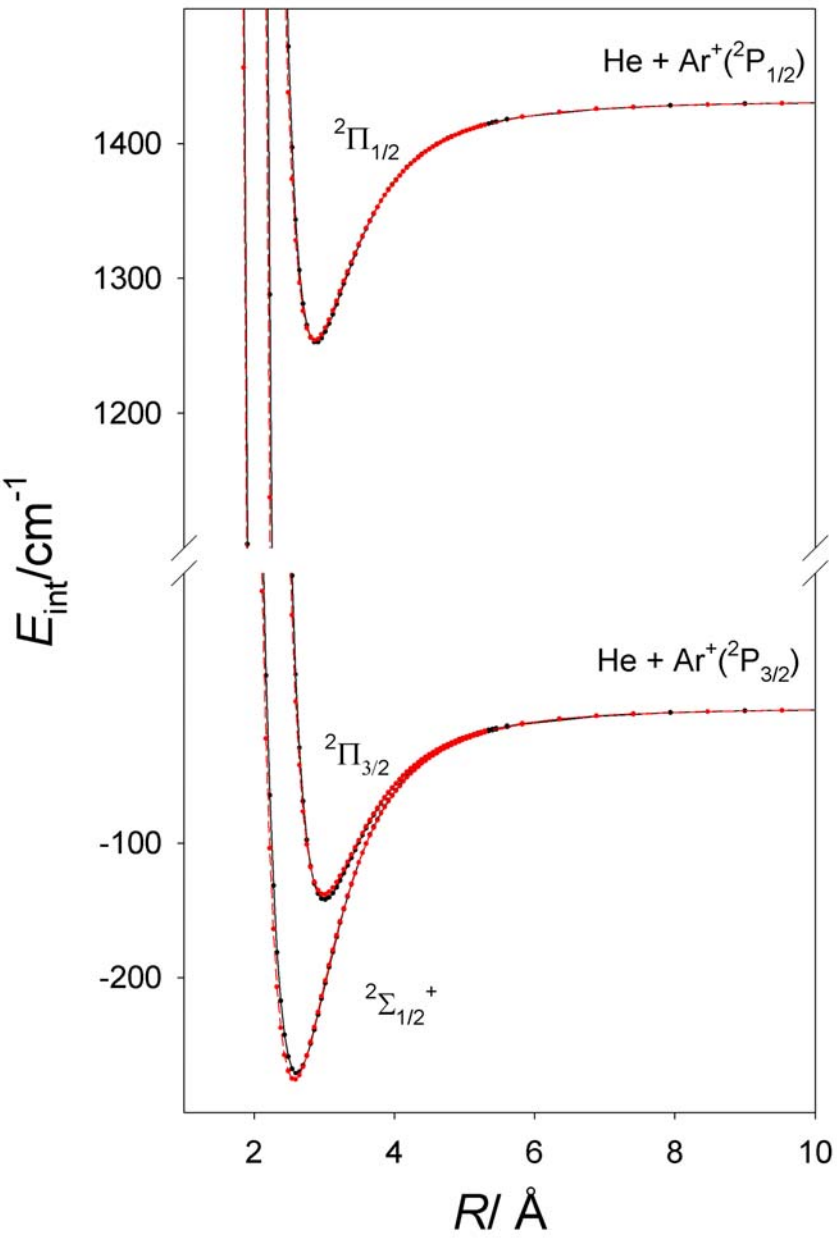
He + Ar+(2P1/2)
2Π1/2
1400
1300
1200
He + Ar+(2P3/2)
2Π3/2
-100
-200
2Σ1/2+
Eint/cm-1
2
4
6
8
10
R/ Å

Figure 2

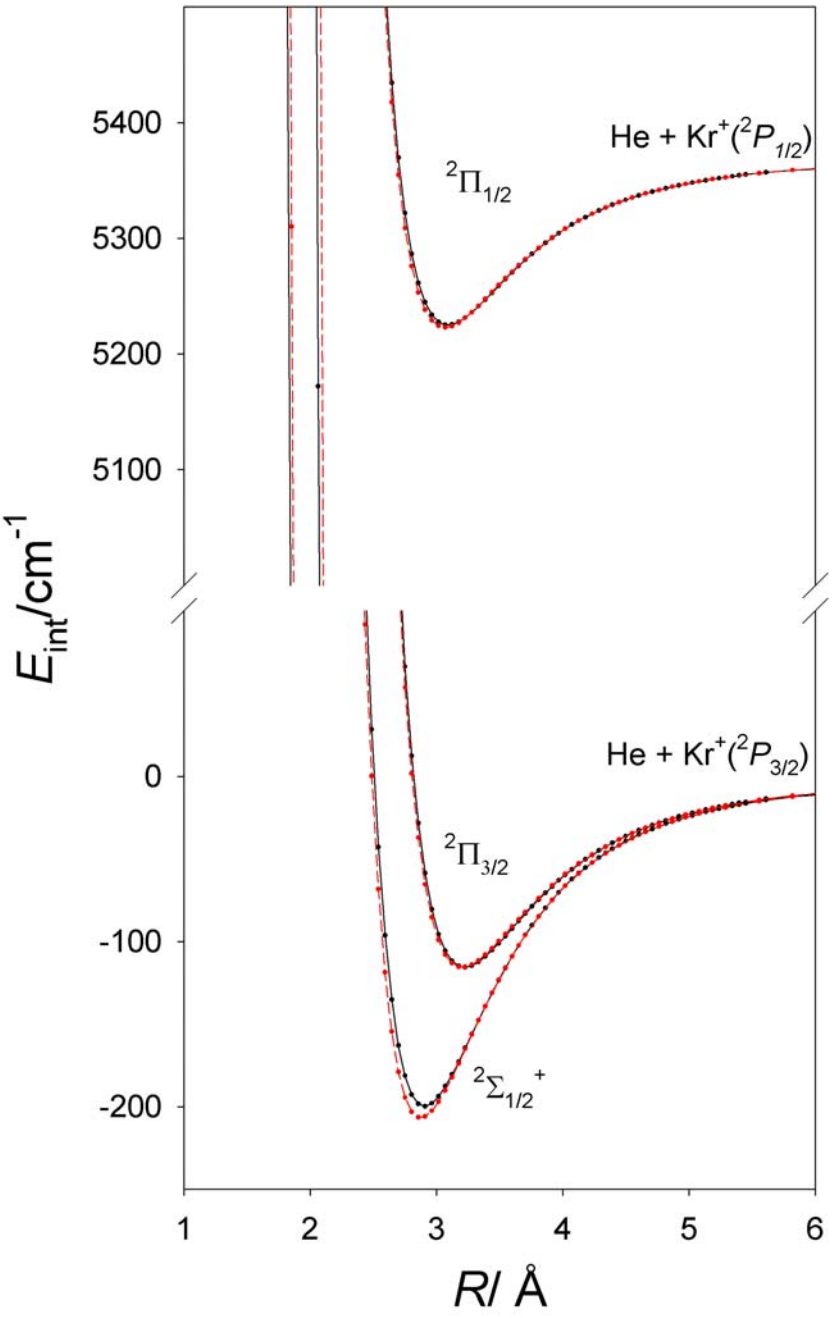
5400
5300
5200
5100
0
-100
-200
1
2
3
4
5
6
E_{int}/cm^{-1}
R/ Å
He + Kr$^+$($^2P_{1/2}$)
$^2\Pi_{1/2}$
He + Kr$^+$($^2P_{3/2}$)
$^2\Pi_{3/2}$
$^2\Sigma_{1/2}^+$

Figure 3

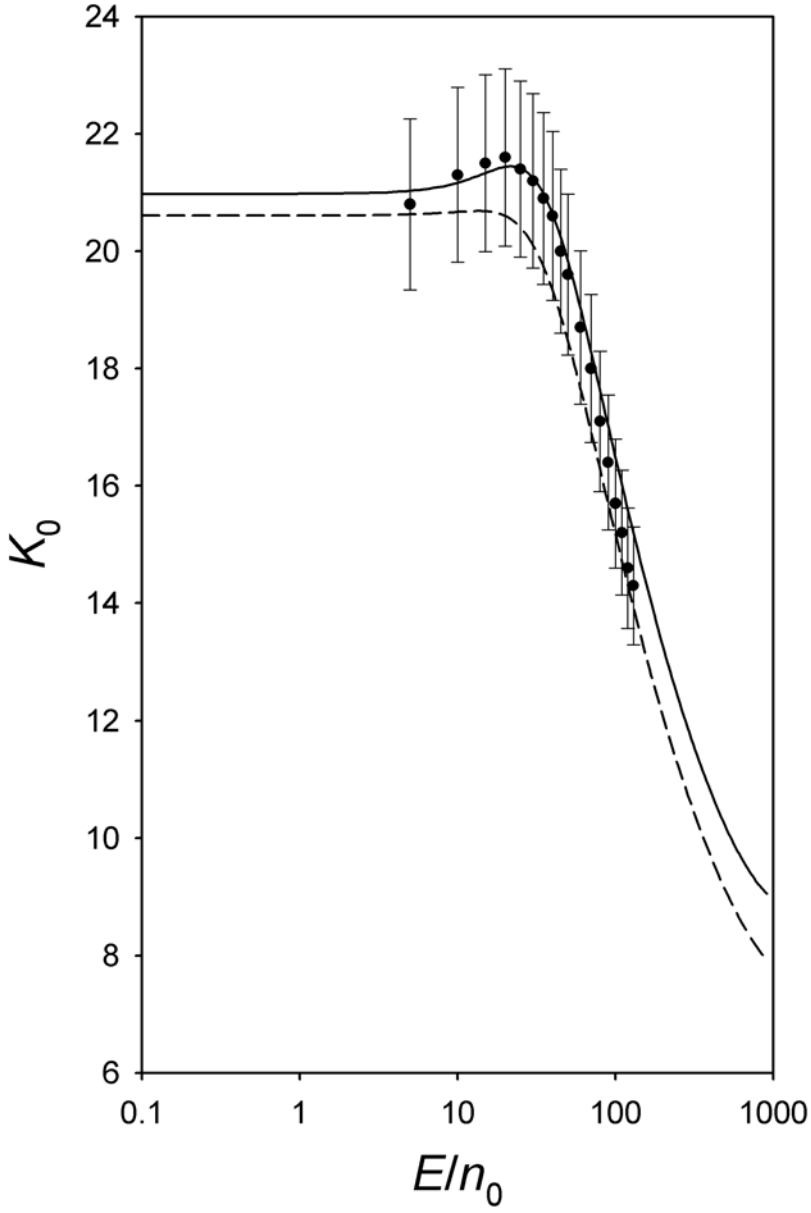

Figure 4

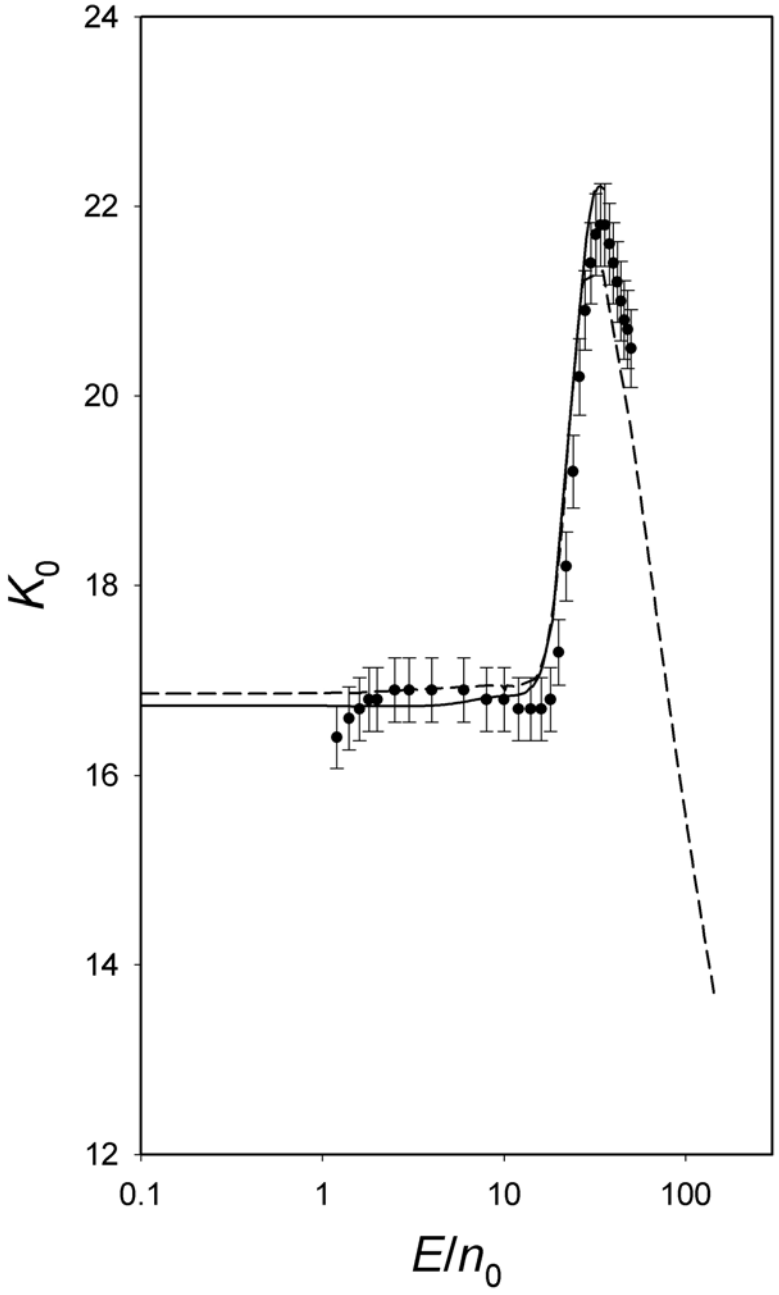

Figure 5

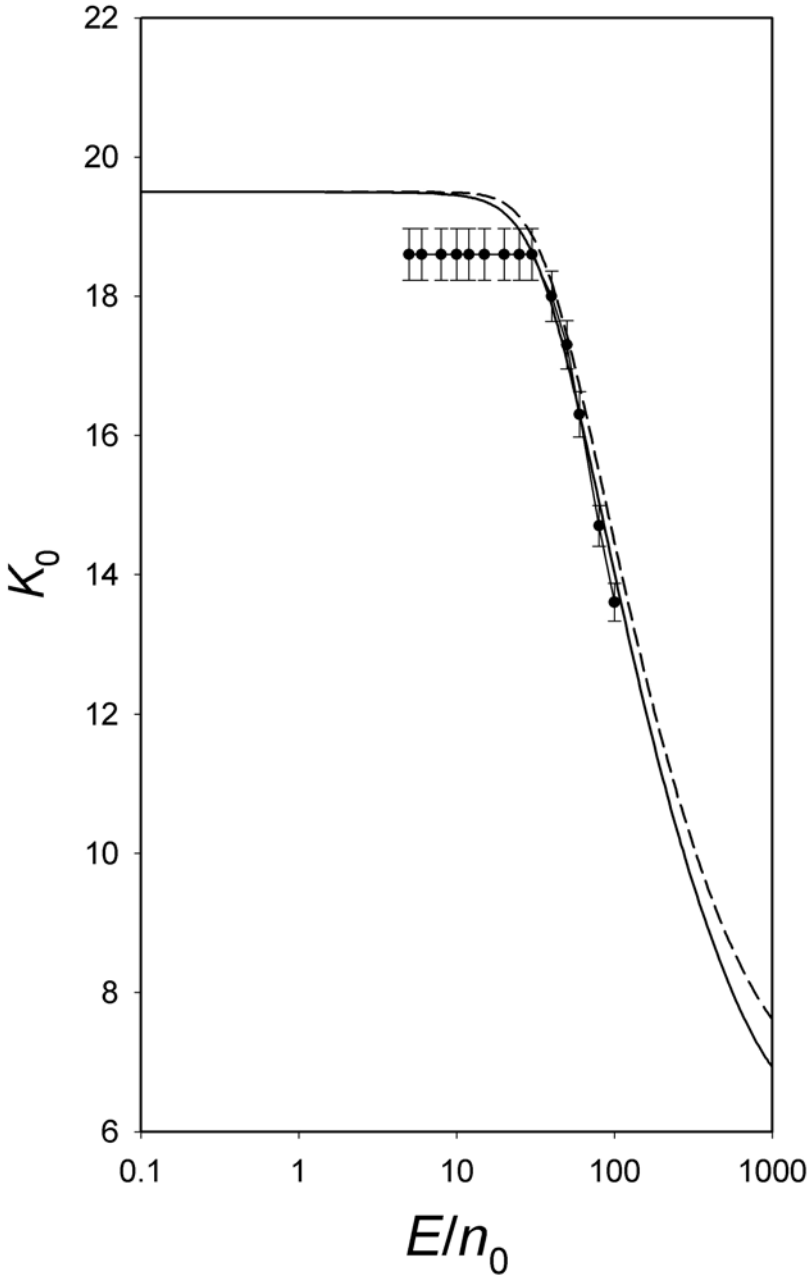

Figure 6

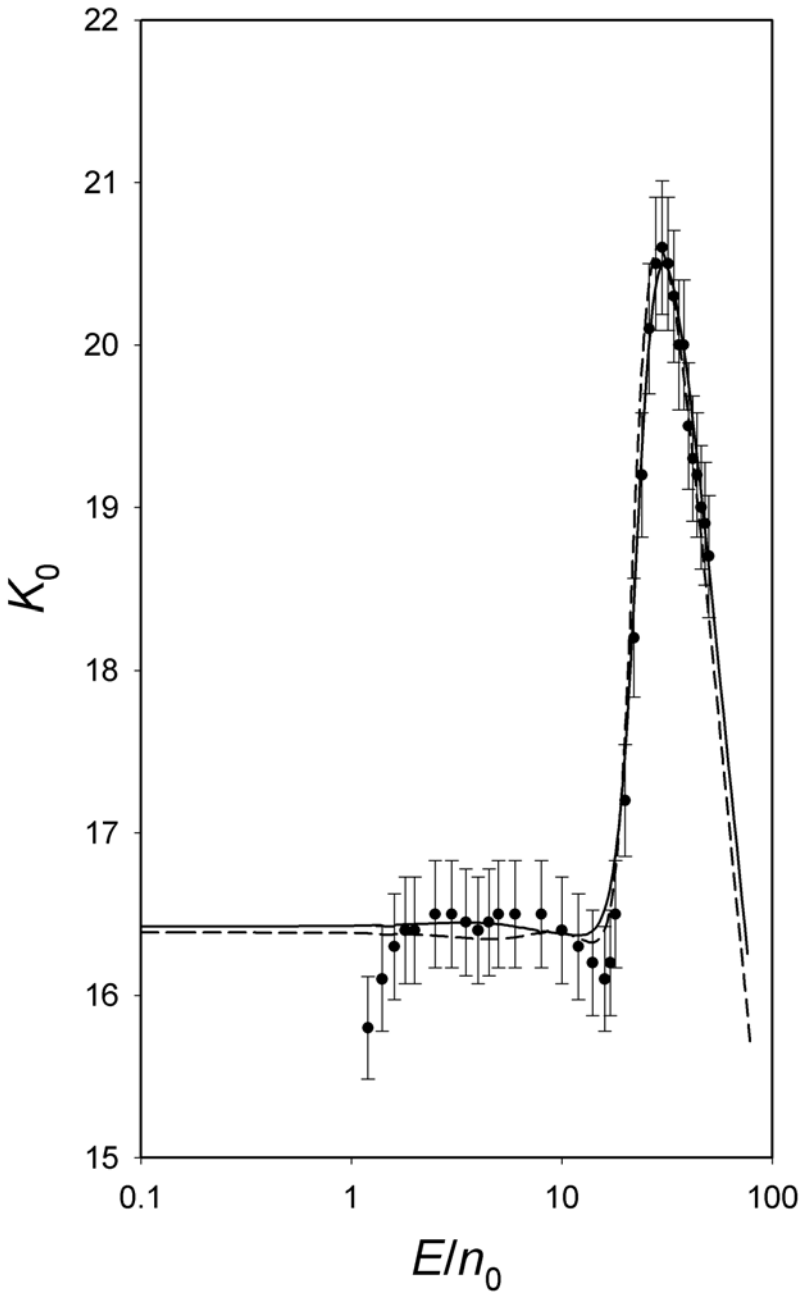

Figure 7

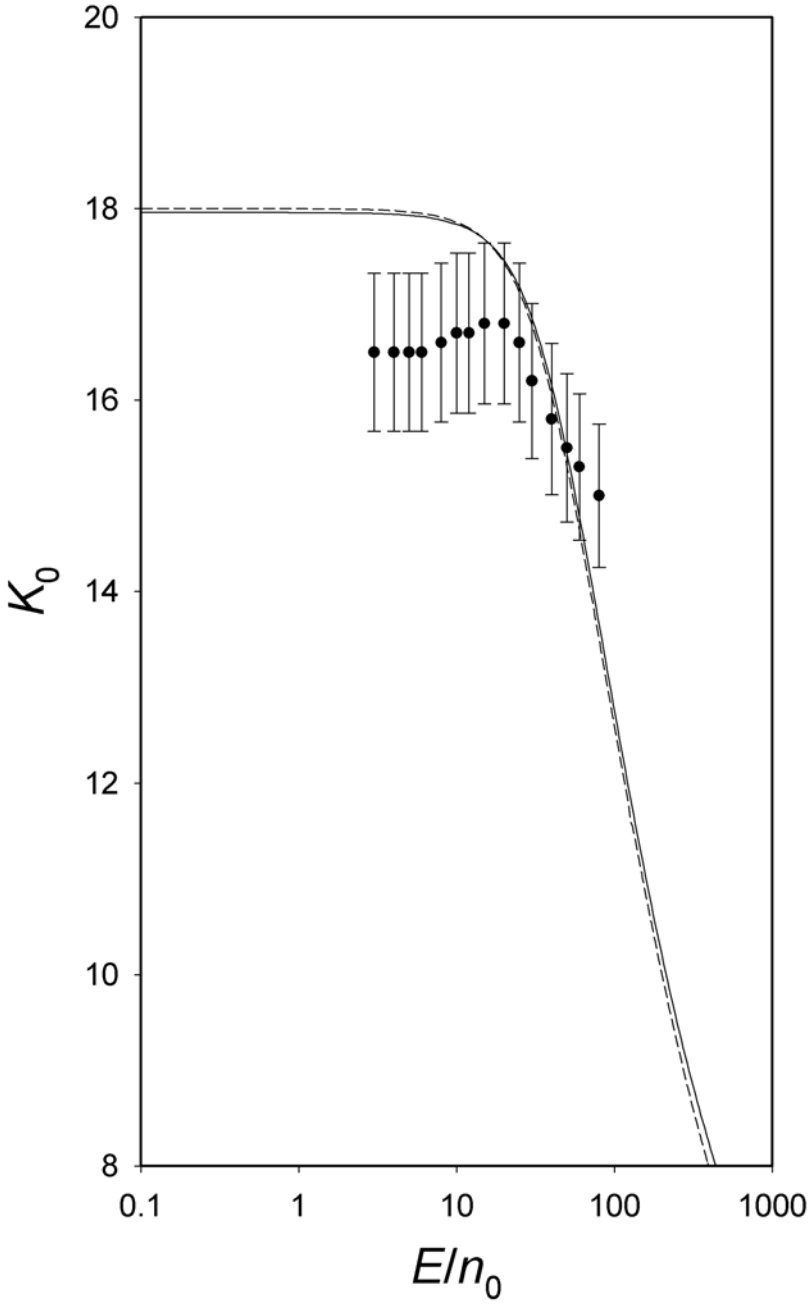

References

[1] T. G. Wright, B. R. Gray, L. A. Viehland and R. J. Johnsen, J. Chem. Phys. 129, 184307 (2008).

[2] I. Dabrowski and G. Herzberg, J. Molec. Spectrosc. 73, 183 (1978).

[3] Y. Tanaka, K. Yoshino and D. E. Freeman, J. Chem. Phys. 62, 4484 (1975).

[4] I. Dabrowski, G. Herzberg and K. Yoshino, J. Molec. Spectrosc.. 89, 491 (1981).

[5] N. Saito, T. M. Kojima, N. Kobayashi and Y. Kaneko, J. Chem. Phys. 100, 5726 (1994).

[6] A. Carrington, C. A. Leach, A. J. Marr, A. M. Shaw, M. R. Viant, J. M. Hutson and M. M. Law, J. Chem. Phys. 102, 2379 (1995).

[7] R. Albat and B. Wirsam, J. Phys. B. At. Molec. Phys. 10, 81 (1977).

[8] V. Sidris, J. C. Brenot, J. Pommier, M. Barat, O. Bernardini, D. C. Lorents and F. T. Smith, J. Phys. B. At. Molec. Phys. 10, 2431 (1977).

[9] R. E. Olson and B. Liu, Chem. Phys. Lett., 56, 537 (1978).

[10] D. Hausamann and H. Morgner, Mol. Phys. 54, 1085 (1985).

[11] P. E. Siska, J. Chem. Phys. 85, 7497 (1986).

[12] D. Stärk and S. D. Peyerimhoff, Molec. Phys. 59, 1241 (1986).

[13] B. Brunetti, F. Vecchiocattivi, A. Aguilar-Navarro and A. Solé, Chem. Phys. Lett. 126, 245 (1986).

[14] K. Balasubramanian, M. Z. Liao and S. H. Lin, Chem. Phys. Lett. 138, 49 (1987).

[15] M. Z. Liao, K. Balasubramanian, D. Chapman and S. H. Lin, Chem. Phys. 111, 423 (1987).

[16] V. Staemmler, Z. Phys. D 16, 167 (1990).

[17] B. Gemein and S. D. Peyerimhoff, Chem. Phys. Lett. 173, 7 (1990).

[18] L. A. Viehland, A. A. Viggiano and E. A. Mason, J. Chem. Phys. 95, 7286 (1991).

[19] N. L. Ma, W.-K. Li and C. Y. Ng, J. Chem. Phys. 99, 3617 (1993).

[20] J. N. Murrell, F. Y. Naumkin and C. R. Griffiths, Molec. Phys. 99, 115 (2001).

[21] N. C. Bera, I. Bhattacharyya and A. K. Das, Int. J. Quant. Chem. 107, 1067 (2006).

[22] H.-P. Weise, Ber. Bunsenges. Phys. Chem. 77, 579 (1973).

[23] K. Balasubramanian, M. Z. Liao and S. H. Lin, Chem. Phys. Lett. 138, 49 (1987).

[24] A. Carrington, C. H. Pyne, A. M. Shaw, S. M. Taylor, J. M. Hutson and M. M. Law, J. Chem. Phys. 105, 8602 (1996).

[25] T. Koizumi, N. Kobayashi and Y. Kaneko, J. Phys. Soc. Jpn, 48, 1678 (1980).

[26] W. Lindinger and D. L. Albritton, J. Chem. Phys. 62, 3517 (1975).

[27] M. J. Hogan, J. Chem. Phys. 125, 164325 (2006)

[28] T. Koizumi, K. Okuno, N. Kobayashi and Y. Kaneko, J. Phys. Soc. Jpn. 51, 2650 (1982) .

[29] T. T. C. Jones, J. D. C. Jones, K. Birkinshaw and N. D. Twiddy, Chem. Phys. Lett. 86, 503 (1982).

[30] R. Johnsen, M. T. Leu and M. A. Biondi, Phys. Rev. A 8, 2557 (1973).

[31] Y. Kaneko, T. Koizumi and N. Kobayashi, Mass Spectrom. (Jpn) 26, 35 (1978).

[32] K.A. Peterson, D. Figgen, E. Goll, H. Stoll and M. Dolg, J. Chem. Phys. 119, 11113 (2003).

[33] MOLPRO is a package of ab initio programs written by H.-J. Werner, P. J. Knowles and others.

[34] See, for example, V. Aquilanti, D. Cappelletti, V. Lorent, E. Luzzatti, and F. Piranti, J. Phys. Chem. 97, 2063 (1993), and references therein.

[35] NIST-JANAF Thermochemical Tables, Ed. M. W. Chase, Jr. (AIP, New York, 1998).

[36] R. J. LeRoy, Level 7.2 – A computer program for solving the radial Schrödinger equation for bound and quasibound levels, and calculating various values and matrix elements. University of Waterloo Chemical Physics Research Program Report CP-555R, 2000.

[37] L. A. Viehland, Chem. Phys. 70, 149 (1982).

[38] L. A. Viehland, Chem. Phys. 85, 291 (1984).

[39] A. Yousef, S. Shrestha, L. A. Viehland, E. P. F. Lee, B. R. Gray, V. L. Ayles, T. G. Wright and W. H. Breckenridge, J. Chem Phys. 127, 154309 (2007).

[40] L. A. Viehland, Chem. Phys. 179, 71 (1994).

[41] To access this database you must telnet to the computer named sassafrass.chatham.edu and logon as gastrans. The required password will be provided upon request by email to viehland@chatham.edu.

[42] M. J. Frisch, G. W. Trucks, H. B. Schlegel, G. E. Scuseria, M. A. Robb, J. R. Cheeseman, J. A. Montgomery, Jr., T. Vreven, K. N. Kudin, J. C. Burant, J. M. Millam, S. S. Iyengar, J. Tomasi, V. Barone, B. Mennucci, M. Cossi, G. Scalmani, N. Rega, G. A. Petersson, H. Nakatsuji, M. Hada, M. Ehara, K. Toyota, R. Fukuda, J. Hasegawa, M. Ishida, T. Nakajima, Y. Honda, O. Kitao, H. Nakai, M. Klene, X. Li, J.

E. Knox, H. P. Hratchian, J. B. Cross, V. Bakken, C. Adamo, J. Jaramillo, R. Gomperts, R. E. Stratmann, O. Yazyev, A. J. Austin, R. Cammi, C. Pomelli, J. Ochterski, P. Y. Ayala, K. Morokuma, G. A. Voth, P. Salvador, J. J. Dannenberg, V. G. Zakrzewski, S. Dapprich, A. D. Daniels, M. C. Strain, O. Farkas, D. K. Malick, A. D. Rabuck, K. Raghavachari, J. B. Foresman, J. V. Ortiz, Q. Cui, A. G. Baboul, S. Clifford, J. Cioslowski, B. B. Stefanov, G. Liu, A. Liashenko, P. Piskorz, I. Komaromi, R. L. Martin, D. J. Fox, T. Keith, M. A. Al-Laham, C. Y. Peng, A. Nanayakkara, M. Challacombe, P. M. W. Gill, B. G. Johnson, W. Chen, M. W. Wong, C. Gonzalez and J. A. Pople, GAUSSIAN 03 (Revision B.03), Gaussian, Inc., Wallingford, CT, 2003.

[43] T. G. Wright, J. Chem. Phys. 105, 7579 (1996).

[44] L. A. Viehland and E. A. Mason, At. Data Nucl. Tables 60, 37 (1995).

[45] H. W. Ellis, M. G. Thackston, E. W. McDaniel and E. A. Mason, At. Data Nucl. Data Tables 31, 113 (1984).

[46] H. W. Ellis, R. Y. Pai, E. W. McDaniel, E. A. Mason and L. A. Viehland, At. Data Nucl. Data Tables 17, 177 (1976).

[47] L. A. Viehland and E. A. Mason, J. Chem. Phys. 99, 1457 (1993).

[48] L. A. Viehland and J. J. Hurly, J. Chem. Phys. 105, 11143 (1996).

[49] T. M. Kojima, N. Saito, N. Kobayashi and Y. Kaneko, J. Phys. Soc. Jpn. 61, 6 (1992).

[50] A. S. Dickinson, J. Phys. B 1, 4687 (1968).

[51] G. Heiche and E. A. Mason, J. Chem. Phys. 53, 387 (1970).

[52] J. Sanderson, H. Tanuma, N. Kobayashi and Y. Kaneko J. Phys. B 26, L465 (1993).

[53] S. Jinno, H. Hidaka, H. Tanuma and N. Kobayashi, XXII ICPEAC, Santa Fe, NM USA (2001).

[54] J. Sanderson, H. Tanuma, N. Kobayashi and Y. Kaneko, J. Phys. B 27, L433 (1994).

[55] H. Hidaka, S. Jinno, H. Tanuma and N. Kobayashi, J. Phys. B 36, 1515 (2003).

[56] H. Hidaka, PhD Thesis, Tokyo Metropolitan University (2003).

[57] K. Ohtsuki, M. Hananoe and M. Matsuzawa, Phys. Rev. Lett. 95, 213201 (2005).

[58] J. Sanderson, H. Tanuma, N. Kobayashi and Y. Kaneko, J. Chem. Phys. 103, 7098 (1995).

[59] H. W. Ellis, E. W. McDaniel, D. L. Albritton, L. A. Viehland, S. L. Lin and E. A. Mason, At. Data Nucl. Data Tables 22, 179 (1978).

[60] D. M. Danailov, L. A. Viehland, R. Johnsen, T. G. Wright, and E. P. F. Lee, J. Chem. Phys. 127, 084303 (2007).

The Supplementary Material consists of an Excel spreadsheet with four worksheets. There is one sheet for each of Ar^+–He, Kr^+–He, Xe^+–He and Rn^+–He. In each sheet, the non-spin-orbit curves for the $^2\Pi$ and $^2\Sigma^+$ states are given, as well as the three spin orbit potentials (see text). Note the units given at the tops of the columns!

R (Bohr)	SIGMA (Ha	PI (Hartree	SIGMA (cm	PI (cm-1)	R (Bohr)	X (cm-1)	V1 (cm-1)	V2 (cm-1)
1.5	0.971199				1.5			
1.6	0.773494				1.6			
1.7	0.620759	1.04432	136240.7	229201.7	1.7	136713	229201.7	230160.8
1.8	0.500106	0.879911	109760.6	193118.2	1.8	110232.3	193118.2	194077.9
1.9	0.403194	0.759758	88490.76	166747.6	1.9	88962.11	166747.6	167707.7
2	0.324521	0.645709	71224.14	141716.7	2	71694.86	141716.7	142677.4
2.1	0.260337	0.546381	57137.38	119916.7	2.1	57607.32	119916.7	120878.2
2.2	0.207943	0.460252	45638.31	101013.7	2.2	46107.3	101013.7	101976.1
2.3	0.165275	0.385949	36273.63	84705.97	2.3	36741.46	84705.97	85669.55
2.4	0.130665	0.322222	28677.68	70719.46	2.4	29144.11	70719.46	71684.44
2.5	0.102725	0.267891	22545.54	58795.17	2.5	23010.29	58795.17	59761.83
2.6	0.080281	0.221833	17619.63	48686.74	2.6	18082.34	48686.74	49655.44
2.7	0.062339	0.182994	13681.83	40162.48	2.7	14142.09	40162.48	41133.64
2.8	0.048062	0.150397	10548.48	33008.36	2.8	11005.78	33008.36	33982.47
2.9	0.036752	0.123159	8066.125	27030.19	2.9	8519.87	27030.19	28007.85
3	0.027828	0.100488	6107.604	22054.57	3	6557.064	22054.57	23036.52
3.1	0.020816	0.081689	4568.529	17928.69	3.1	5012.838	17928.69	18915.79
3.2	0.015327	0.066155	3363.89	14519.31	3.2	3802.016	14519.31	15512.6
3.3	0.011049	0.053361	2424.964	11711.4	3.3	2855.687	11711.4	12712.08
3.4	0.00773	0.042858	1696.532	9406.266	3.4	2118.426	9406.266	10415.78
3.5	0.005169	0.034263	1134.456	7519.894	3.5	1545.874	7519.894	8539.886
3.6	0.003206	0.027252	703.594	5981.096	3.6	1102.668	5981.096	7013.433
3.7	0.001713	0.021551	376.0369	4729.858	3.7	760.6937	4729.858	5776.611
3.8	0.000591	0.01693	129.6568	3715.798	3.8	497.6672	3715.798	4779.197
3.9	-0.000242	0.013199	-53.07774	2896.791	3.9	295.9834	2896.791	3979.14
4	-0.000848	0.010196	-186.0574	2237.748	4	141.805	2237.748	3341.296
4.1	-0.001277	0.007789	-280.2779	1709.536	4.1	24.35397	1709.536	2836.314
4.2	-0.001569	0.005869	-344.461	1288.015	4.2	-64.6902	1288.015	2439.655
4.3	-0.001757	0.004343	-385.516	953.2551	4.3	-131.6633	953.2551	2130.812
4.4	-0.001863	0.003138	-408.912	688.8058	4.4	-181.3439	688.8058	1892.648
4.5	-0.001909	0.002192	-418.9749	481.152	4.5	-217.3291	481.152	1710.916
4.6	-0.00191	0.001454	-419.1175	319.2061	4.6	-242.3557	319.2061	1573.854
4.7	-0.001877	0.000884	-412.0219	193.9102	4.7	-258.555	193.9102	1471.853
4.8	-0.001822	0.000446	-399.7928	97.87471	4.8	-267.6479	97.87471	1397.14
4.9	-0.00175	0.000114	-384.0521	25.1057	4.9	-271.0465	25.1057	1343.51
5	-0.001668	-0.000133	-366.0464	-29.24938	5	-269.9408	-29.24938	1306.055
5.1	-0.00158	-0.000315	-346.7611	-69.10378	5.1	-265.3687	-69.10378	1280.914
5.2	-0.001489	-0.000445	-326.9009	-97.60037	5.2	-258.1769	-97.60037	1265.086
5.3	-0.001399	-0.000534	-307.0055	-117.2587	5.3	-249.0905	-117.2587	1256.236
5.4	-0.00131	-0.000593	-287.4591	-130.0848	5.4	-238.7008	-130.0848	1252.567
5.5	-0.001224	-0.000627	-268.536	-137.672	5.5	-227.4902	-137.672	1252.692
5.6	-0.001141	-0.000644	-250.4227	-141.2846	5.6	-215.8445	-141.2846	1255.547
5.7	-0.001063	-0.000647	-233.2335	-141.9189	5.7	-204.0617	-141.9189	1260.319
5.8	-0.000989	-0.00064	-217.0341	-140.354	5.8	-192.3703	-140.354	1266.392
5.9	-0.00092	-0.000625	-201.8508	-137.2068	5.9	-180.9417	-137.2068	1273.294
6	-0.000855	-0.000606	-187.6793	-132.9511	6	-169.8956	-132.9511	1280.675
6.1	-0.000795	-0.000583	-174.4933	-127.9559	6.1	-159.3134	-127.9559	1288.274
6.2	-0.000739	-0.000558	-162.2598	-122.502	6.2	-149.2503	-122.502	1295.899
6.3	-0.000688	-0.000532	-150.9327	-116.8066	6.3	-139.7367	-116.8066	1303.407
6.4	-0.00064	-0.000506	-140.4638	-111.0256	6.4	-130.7847	-111.0256	1310.705
6.5	-0.000596	-0.00048	-130.7937	-105.2798	6.5	-122.3895	-105.2798	1317.726

6.6	-0.000555	-0.000454	-121.8721	-99.65246	6.6	-114.5418	-99.65246	1324.427
6.7	-0.000518	-0.000429	-113.6396	-94.2029	6.7	-107.2191	-94.2029	1330.787
6.8	-0.000483	-0.000405	-106.0633	-88.97063	6.8	-100.4109	-88.97063	1336.787
6.9	-0.000451	-0.000383	-99.05987	-83.97977	6.9	-94.06835	-83.97977	1342.439
7	-0.000422	-0.000361	-92.60732	-79.24132	7	-88.17963	-79.24132	1347.741
7.1	-0.000395	-0.000341	-86.65297	-74.75964	7.1	-82.71043	-74.75964	1352.708
7.2	-0.00037	-0.000321	-81.15513	-70.53256	7.2	-77.63175	-70.53256	1357.354
7.3	-0.000347	-0.000303	-76.07649	-66.55349	7.3	-72.9162	-66.55349	1361.696
7.4	-0.000325	-0.000286	-71.38632	-62.81583	7.4	-68.54087	-62.81583	1365.749
7.5	-0.000305	-0.00027	-67.04511	-59.30643	7.5	-64.47483	-59.30643	1369.533
7.6	-0.000287	-0.000255	-63.03311	-56.01651	7.6	-60.70188	-56.01651	1373.062
7.7	-0.00027	-0.000241	-59.31082	-52.93509	7.7	-57.19188	-52.93509	1376.356
7.8	-0.000255	-0.000228	-55.86727	-50.0468	7.8	-53.93236	-50.0468	1379.428
7.9	-0.00024	-0.000216	-52.66733	-47.34068	7.9	-50.89618	-47.34068	1382.298
8	-0.000226	-0.000204	-49.69784	-44.80794	8	-48.07158	-44.80794	1384.976
8.1	-0.000214	-0.000193	-46.93684	-42.43761	8.1	-45.44024	-42.43761	1387.476
8.2	-0.000202	-0.000183	-44.3668	-40.21653	8.2	-42.98605	-40.21653	1389.813
8.3	-0.000191	-0.000174	-41.97233	-38.13811	8.3	-40.69653	-38.13811	1391.996
8.5	-0.000172	-0.000157	-37.65965	-34.36095	8.5	-36.56177	-34.36095	1395.951
8.6	-0.000163	-0.000149	-35.71291	-32.64905	8.6	-34.69308	-32.64905	1397.741
8.7	-0.000154	-0.000141	-33.89347	-31.0403	8.7	-32.94367	-31.0403	1399.42
8.9	-0.000139	-0.000128	-30.58868	-28.11199	8.9	-29.76407	-28.11199	1402.473
9	-0.000133	-0.000122	-29.09874	-26.77769	9	-28.3259	-26.77769	1403.859
9.1	-0.000126	-0.000116	-27.69588	-25.5221	9.1	-26.97202	-25.5221	1405.164
9.3	-0.000115	-0.000106	-25.13737	-23.22511	9.3	-24.50052	-23.22511	1407.548
9.4	-0.000109	-0.000101	-23.97063	-22.17405	9.4	-23.37227	-22.17405	1408.638
9.5	-0.000104	-9.65E-05	-22.87042	-21.18226	9.5	-22.30814	-21.18226	1409.665
9.7	-9.5E-05	-8.82E-05	-20.85945	-19.36094	9.7	-20.3603	-19.36094	1411.55
9.8	-9.08E-05	-8.44E-05	-19.93276	-18.52451	9.8	-19.46365	-18.52451	1412.416
9.9	-8.69E-05	-8.08E-05	-19.06834	-17.73361	9.9	-18.62371	-17.73361	1413.232
10.1	-7.95E-05	-7.42E-05	-17.45437	-16.27675	10.1	-17.06205	-16.27675	1414.741
10.2	-7.62E-05	-7.11E-05	-16.72981	-15.60581	10.2	-16.35534	-15.60581	1415.43
10.3	-7.3E-05	-6.82E-05	-16.02108	-14.97019	10.3	-15.67095	-14.97019	1416.09
10.6	-6.45E-05	-6.04E-05	-14.15249	-13.25399	10.6	-13.85312	-13.25399	1417.857
11	-5.49E-05	-5.17E-05	-12.05844	-11.34338	11	-11.82016	-11.34338	1419.828
13	-2.7E-05	-2.59E-05	-5.922238	-5.688253	13	-5.844251	-5.688253	1425.644
15	-1.48E-05	-1.44E-05	-3.243847	-3.154161	15	-3.213953	-3.154161	1428.226
17	-8.86E-06	-8.6E-06	-1.945034	-1.888348	17	-1.926139	-1.888348	1429.503
20	-4.57E-06	-4.44E-06	-1.003242	-0.975325	20	-0.993936	-0.975325	1430.425
25	-1.84E-06	-1.81E-06	-0.403401	-0.397678	25	-0.401494	-0.397678	1431.01
30	-8.65E-07	-8.79E-07	-0.189884	-0.192901	30	-0.190889	-0.192901	1431.218
40	-3.3E-07	-2.89E-07	-0.072404	-0.063373	40	-0.069393	-0.063373	1431.344

R (Bohr)	SIGMA (Ha	PI (Hartree	SIGMA (cm	PI (cm-1)	R (Bohr)	X (cm-1)	V1 (cm-1)	V2 (cm-1)
1.5	1.53087				1.5			
1.6	1.206861				1.6			
1.7	0.95986				1.7			
1.8	0.768867	0.984674	168746.9	216111	1.8	170407.1	216111	219821.8
1.9	0.619182				1.9			
2	0.500441	0.824559	109834.1	180969.8	2	111536.6	180969.8	184638.2
2.1	0.405279	0.700283	88948.51	153694.3	2.1	90642.64	153694.3	157371.2
2.2	0.328413	0.594032	72078.34	130375	2.2	73762.18	130375	134062.1
2.3	0.265989	0.503048	58377.88	110406.2	2.3	60049.36	110406.2	114105.8
2.4	0.215135	0.425042	47216.68	93285.89	2.4	48873.44	93285.89	97000.12
2.5	0.173653	0.358196	38112.37	78614.97	2.5	39751.67	78614.97	82346.68
2.6	0.139818	0.301016	30686.51	66065.28	2.6	32305.17	66065.28	69817.63
2.7	0.112249	0.252227	24635.72	55357.41	2.7	26230.05	55357.41	59134.08
2.8	0.08982	0.210721	19713.16	46247.97	2.8	21278.95	46247.97	50053.18
2.9	0.071608	0.175521	15716.03	38522.48	2.9	17248.44	38522.48	42361.07
3	0.05685	0.145763	12477.03	31991.28	3	13970.59	31991.28	35868.71
3.1	0.044916	0.120683	9857.914	26486.86	3.1	11306.55	26486.86	30409.22
3.2	0.035288	0.09961	7744.711	21861.95	3.2	9141.777	21861.95	25835.88
3.3	0.027536	0.081957	6043.543	17987.54	3.3	7381.988	17987.54	22020.09
3.4	0.021312	0.067212	4677.384	14751.37	3.4	5949.985	14751.37	18849.77
3.5	0.016326	0.054931	3583.123	12056.02	3.5	4782.829	12056.02	16227.32
3.6	0.012344	0.044732	2709.258	9817.506	3.6	3829.627	9817.506	14068.14
3.7	0.009175	0.036285	2013.781	7963.655	3.7	3049.47	7963.655	12298.97
3.8	0.006664	0.02931	1462.537	6432.731	3.8	2409.774	6432.731	10856.49
3.9	0.004683	0.023566	1027.725	5172.152	3.9	1884.678	5172.152	9686.199
4	0.003129	0.018851	686.7932	4137.261	4	1453.754	4137.261	8741.301
4.1	0.00192	0.014992	421.4088	3290.259	4.1	1100.755	3290.259	7981.913
4.2	0.000987	0.011843	216.6851	2599.227	4.2	812.6317	2599.227	7374.281
4.3	0.000276	0.009283	60.54647	2037.365	4.3	578.7552	2037.365	6890.156
4.4	-0.000259	0.007209	-56.8132	1582.116	4.4	390.2849	1582.116	6506.018
4.5	-0.000653	0.005534	-143.3477	1214.681	4.5	239.7856	1214.681	6202.548
4.6	-0.000936	0.004189	-205.4941	919.3112	4.6	120.92	919.3112	5963.897
4.7	-0.001132	0.003112	-248.465	682.964	4.7	28.27831	682.964	5777.221
4.8	-0.00126	0.002254	-276.4722	494.7704	4.8	-42.78013	494.7704	5632.078
4.9	-0.001335	0.001576	-292.8977	345.7833	4.9	-96.19083	345.7833	5520.076
5	-0.001369	0.001042	-300.4674	228.5894	5	-135.3051	228.5894	5434.427
5.1	-0.001373	0.000625	-301.3518	137.1255	5.1	-162.9259	137.1255	5369.7
5.2	-0.001355	0.000302	-297.2806	66.38669	5.2	-181.4041	66.38669	5321.51
5.3	-0.00132	5.6E-05	-289.6209	12.29758	5.3	-192.681	12.29758	5286.358
5.4	-0.001273	-0.00013	-279.4483	-28.47903	5.4	-198.3567	-28.47903	5261.429
5.5	-0.001219	-0.000267	-267.6032	-58.66518	5.5	-199.7397	-58.66518	5244.471
5.6	-0.001161	-0.000367	-254.7332	-80.46818	5.6	-197.8876	-80.46818	5233.686
5.7	-0.0011	-0.000436	-241.3343	-95.68004	5.7	-193.6526	-95.68004	5227.638
5.8	-0.001038	-0.000482	-227.7817	-105.7451	5.8	-187.7143	-105.7451	5225.188
5.9	-0.000977	-0.00051	-214.3521	-111.8272	5.9	-180.6092	-111.8272	5225.43
6	-0.000917	-0.000523	-201.2473	-114.8555	6	-172.7571	-114.8555	5227.654
6.1	-0.000859	-0.000527	-188.6077	-115.5715	6.1	-164.482	-115.5715	5231.303
6.2	-0.000804	-0.000522	-176.5388	-114.5636	6.2	-156.0387	-114.5636	5235.936
6.3	-0.000752	-0.000512	-165.0713	-112.2902	6.3	-147.5925	-112.2902	5241.231
6.4	-0.000703	-0.000497	-154.2534	-109.1184	6.4	-139.2924	-109.1184	5246.921
6.5	-0.000657	-0.00048	-144.0917	-105.3279	6.5	-131.2324	-105.3279	5252.813

6.6	-0.000613	-0.000461	-134.5796	-101.1383	6.6	-123.4787	-101.1383	5258.761
6.7	-0.000573	-0.000441	-125.7019	-96.71571	6.7	-116.0745	-96.71571	5264.657
6.8	-0.000535	-0.00042	-117.4365	-92.18812	6.8	-109.0467	-92.18812	5270.422
6.9	-0.0005	-0.000399	-109.7505	-87.65122	6.9	-102.4042	-87.65122	5276.003
7	-0.000468	-0.000379	-102.6154	-83.1743	7	-96.15063	-83.1743	5281.361
7.1	-0.000437	-0.000359	-95.99381	-78.80966	7.1	-90.27797	-78.80966	5286.474
7.2	-0.000409	-0.00034	-89.8595	-74.59284	7.2	-84.78025	-74.59284	5291.328
7.3	-0.000384	-0.000321	-84.17291	-70.54542	7.3	-79.63809	-70.54542	5295.92
7.4	-0.00036	-0.000304	-78.90113	-66.68517	7.4	-74.83531	-66.68517	5300.249
7.5	-0.000337	-0.000287	-74.02001	-63.01775	7.5	-70.3576	-63.01775	5304.32
7.6	-0.000317	-0.000271	-69.49225	-59.54786	7.6	-66.18154	-59.54786	5308.141
7.7	-0.000298	-0.000256	-65.2959	-56.27549	7.7	-62.29246	-56.27549	5311.721
7.8	-0.00028	-0.000242	-61.40461	-53.19187	7.8	-58.66982	-53.19187	5315.073
7.9	-0.000263	-0.000229	-57.79206	-50.29481	7.9	-55.2953	-50.29481	5318.208
8	-0.000248	-0.000217	-54.43849	-47.57552	8	-52.15278	-47.57552	5321.139
8.1	-0.000234	-0.000205	-51.32195	-45.02522	8.1	-49.22468	-45.02522	5323.878
8.2	-0.000221	-0.000194	-48.42488	-42.63514	8.2	-46.49636	-42.63514	5326.436
8.3	-0.000208	-0.000184	-45.72973	-40.39431	8.3	-43.95244	-40.39431	5328.828
8.5	-0.000186	-0.000166	-40.87934	-36.33183	8.5	-39.36436	-36.33183	5333.153
8.6	-0.000176	-0.000157	-38.69777	-34.48824	8.6	-37.29533	-34.48824	5335.109
8.7	-0.000167	-0.000149	-36.66324	-32.75878	8.7	-35.36238	-32.75878	5336.94
8.8	-0.000158	-0.000142	-34.76039	-31.13687	8.8	-33.55309	-31.13687	5338.656
8.9	-0.00015	-0.000135	-32.98202	-29.61468	8.9	-31.86004	-29.61468	5340.263
9	-0.000143	-0.000128	-31.31858	-28.18304	9	-30.27381	-28.18304	5341.772
9.1	-0.000136	-0.000122	-29.75857	-26.83698	9.1	-28.78506	-26.83698	5343.19
9.3	-0.000123	-0.000111	-26.92826	-24.37648	9.3	-26.07793	-24.37648	5345.773
9.4	-0.000117	-0.000106	-25.64143	-23.25118	9.4	-24.84492	-23.25118	5346.952
9.5	-0.000111	-0.000101	-24.43234	-22.1909	9.5	-23.6854	-22.1909	5348.062
9.7	-0.000101	-9.22E-05	-22.22482	-20.24481	9.7	-21.56498	-20.24481	5350.095
9.8	-9.67E-05	-8.82E-05	-21.21598	-19.35168	9.8	-20.59469	-19.35168	5351.027
9.9	-9.23E-05	-8.43E-05	-20.26603	-18.50816	9.9	-19.6802	-18.50816	5351.906
10.1	-8.44E-05	-7.73E-05	-18.52235	-16.95562	10.1	-18.00021	-16.95562	5353.522
10.2	-8.07E-05	-7.4E-05	-17.72206	-16.24097	10.2	-17.22845	-16.24097	5354.265
10.3	-7.73E-05	-7.09E-05	-16.96646	-15.56471	10.3	-16.49929	-15.56471	5354.968
10.6	-6.8E-05	-6.26E-05	-14.92992	-13.7406	10.6	-14.53354	-13.7406	5356.863
11	-5.77E-05	-5.34E-05	-12.6743	-11.71487	11	-12.35453	-11.71487	5358.965
13	-2.8E-05	-2.64E-05	-6.135025	-5.799921	13	-6.023328	-5.799921	5365.088
15	-1.52E-05	-1.46E-05	-3.340628	-3.20365	15	-3.294969	-3.20365	5367.751
17	-9.02E-06	-8.73E-06	-1.979413	-1.914992	17	-1.95794	-1.914992	5369.064
20	-4.61E-06	-4.51E-06	-1.012619	-0.988985	20	-1.004741	-0.988985	5370.003
25	-1.87E-06	-1.83E-06	-0.409457	-0.402579	25	-0.407164	-0.402579	5370.595
30	-9.03E-07	-8.92E-07	-0.198253	-0.195697	30	-0.197401	-0.195697	5370.803
40	-3.01E-07	-2.99E-07	-0.066036	-0.065542	40	-0.065871	-0.065542	5370.934

R (Bohr)	SIGMA (Ha	PI (Hartree	SIGMA (cm	PI (cm-1)	R (Bohr)	X (cm-1)	V1 (cm-1)	V2 (cm-1)
2	1.027011		225402.9	0				
2.1	0.835373	1.0853	183343.2	238195.7	2.1	190534.1	238195.7	261899.9
2.2	0.681153	0.889625	149495.8	195250	2.2	156235.9	195250	219405
2.3	0.556505	0.781772	122138.7	171579	2.3	129075.5	171579	195537.3
2.4	0.455442	0.664318	99957.9	145801.1	2.4	106703	145801.1	169951.1
2.5	0.373281	0.565291	81925.79	124067.1	2.5	88450.78	124067.1	148437.2
2.6	0.306301	0.48144	67225.22	105663.9	2.6	73503.07	105663.9	130281.2
2.7	0.251533	0.410143	55205.1	90015.97	2.7	61209.93	90015.97	114906.2
2.8	0.206624	0.349311	45348.76	76664.83	2.8	51056.45	76664.83	101852.2
2.9	0.169712	0.297283	37247.56	65245.98	2.9	42636.6	65245.98	90752.04
3	0.139321	0.252725	30577.32	55466.71	3	35629.74	55466.71	81309.38
3.1	0.114268	0.214548	25078.92	47087.81	3.1	29781.15	47087.81	73280.69
3.2	0.093603	0.181845	20543.49	39910.33	3.2	24887	39910.33	66461.93
3.3	0.076552	0.153851	16801.31	33766.37	3.3	20783.05	33766.37	60679.73
3.4	0.062485	0.129914	13713.78	28512.82	3.4	17336.32	28512.82	55785.39
3.5	0.050881	0.109474	11167.15	24026.83	3.5	14438.45	24026.83	51650.63
3.6		0.092049	0	20202.36				
3.7	0.033437	0.077219	7338.626	16947.63	3.7	9950.14	16947.63	45231.21
3.8	0.026954	0.064622	5915.675	14182.96	3.8	8225.98	14182.96	42767.76
3.9	0.021625	0.053944	4746.156	11839.26	3.9	6777.697	11839.26	40702.82
4	0.017252	0.044909	3786.352	9856.492	4	5562.844	9856.492	38975.1
4.1	0.013669	0.037283	3000.018	8182.594	4.1	4545.597	8182.594	37532.12
4.2	0.01074	0.030858	2357.131	6772.491	4.2	3695.617	6772.491	36329.11
4.3	0.008351	0.025457	1832.806	5587.236	4.3	2987.136	5587.236	35328.01
4.4	0.006408	0.020928	1406.391	4593.227	4.4	2398.204	4593.227	34496.51
4.5	0.004833	0.017139	1060.813	3761.563	4.5	1910.165	3761.563	33807.31
4.6	0.003562	0.013976	781.8476	3067.408	4.6	1507.074	3067.408	33237.28
4.7	0.002541	0.011343	557.7772	2489.499	4.7	1175.414	2489.499	32766.96
4.8	0.001726	0.009157	378.7825	2009.635	4.8	903.6114	2009.635	32379.91
4.9	0.001079	0.007346	236.8043	1612.3	4.9	681.899	1612.3	32062.31
5	0.00057	0.005851	125.094	1284.24	5	501.934	1284.24	31802.5
5.1	0.000174	0.004621	38.0986	1014.269	5.1	356.7076	1014.269	31590.76
5.2	-0.000131	0.003612	-28.79946	792.8104	5.2	240.2585	792.8104	31418.85
5.3	-0.000362	0.002788	-79.45201	611.825	5.3	147.5623	611.825	31279.91
5.4	-0.000533	0.002116	-116.9493	464.4895	5.4	74.44734	464.4895	31168.19
5.5	-0.000656	0.001572	-143.9183	345.0887	5.5	17.37317	345.0887	31078.9
5.6	-0.00074	0.001134	-162.4968	248.7921	5.6	-26.61183	248.7921	31008.01
5.7	-0.000795	0.000782	-174.434	171.5685	5.7	-59.95773	171.5685	30952.19
5.8	-0.000825	0.000501	-181.1631	110.038	5.8	-84.70411	110.038	30908.68
5.9	-0.000838	0.00028	-183.8495	61.37461	5.9	-102.5395	61.37461	30875.16
6	-0.000836	0.000106	-183.4391	23.24017	6	-114.8526	23.24017	30849.75
6.1	-0.000823	-2.88E-05	-180.6913	-6.31656	6.1	-122.7847	-6.31656	30830.88
6.2	-0.000803	-0.000132	-176.225	-28.90481	6.2	-127.2741	-28.90481	30817.24
6.3	-0.000777	-0.000209	-170.5274	-45.8733	6.3	-129.0876	-45.8733	30807.79
6.4	-0.000747	-0.000266	-163.9871	-58.30782	6.4	-128.8409	-58.30782	30801.65
6.5	-0.000715	-0.000306	-156.9112	-67.13289	6.5	-127.043	-67.13289	30798.1
6.6	-0.000681	-0.000333	-149.5346	-73.07188	6.6	-124.0891	-73.07188	30796.58
6.7	-0.000647	-0.00035	-142.0418	-76.75128	6.7	-120.3089	-76.75128	30796.62
6.8	-0.000613	-0.000358	-134.5731	-78.64873	6.8	-115.9541	-78.64873	30797.83
6.9	-0.00058	-0.000361	-127.2316	-79.18001	6.9	-111.231	-79.18001	30799.92
7	-0.000547	-0.000358	-120.0943	-78.65751	7	-106.2944	-78.65751	30802.64

7.1	-0.000516	-0.000352	-113.216	-77.35134	7.1	-101.2704	-77.35134	30805.8
7.2	-0.000486	-0.000344	-106.6296	-75.46635	7.2	-96.2488	-75.46635	30809.25
7.3	-0.000457	-0.000333	-100.3592	-73.1702	7.3	-91.30149	-73.1702	30812.87
7.4	-0.00043	-0.000322	-94.4136	-70.59401	7.4	-86.47782	-70.59401	30816.57
7.5	-0.000405	-0.000309	-88.79944	-67.83833	7.5	-81.81556	-67.83833	30820.28
7.6	-0.000381	-0.000296	-83.5101	-64.98644	7.6	-77.33801	-64.98644	30823.94
7.7	-0.000358	-0.000283	-78.539	-62.09781	7.7	-73.06054	-62.09781	30827.52
7.8	-0.000337	-0.00027	-73.87736	-59.22084	7.8	-68.99339	-59.22084	30831
7.9	-0.000317	-0.000257	-69.50981	-56.38781	7.9	-65.13705	-56.38781	30834.34
8	-0.000298	-0.000244	-65.42539	-53.62643	8	-61.4934	-53.62643	30837.54
8.1	-0.000281	-0.000232	-61.60653	-50.95542	8.1	-58.05698	-50.95542	30840.6
8.2	-0.000264	-0.00022	-58.04007	-48.38757	8.2	-54.82324	-48.38757	30843.5
8.3	-0.000249	-0.000209	-54.70844	-45.92726	8.3	-51.78194	-45.92726	30846.25
8.5	-0.000222	-0.000188	-48.69703	-41.34902	8.5	-46.24808	-41.34902	30851.3
8.6	-0.00021	-0.000179	-45.98652	-39.23548	8.6	-43.7365	-39.23548	30853.61
8.7	-0.000198	-0.00017	-43.45598	-37.23168	8.7	-41.38149	-37.23168	30855.79
8.9	-0.000177	-0.000153	-38.88663	-33.55652	8.9	-37.11013	-33.55652	30859.77
9	-0.000168	-0.000145	-36.82221	-31.87047	9	-35.17181	-31.87047	30861.58
9.1		-0.000138	0	-30.28544	9.1			
9.3	-0.000143	-0.000125	-31.39849	-27.38375	9.3	-30.06036	-27.38375	30866.38
9.4	-0.000136	-0.000119	-29.81403	-26.05726	9.4	-28.56187	-26.05726	30867.79
9.5	-0.000129	-0.000113	-28.33109	-24.81229	9.5	-27.15825	-24.81229	30869.11
9.8	-0.000111	-0.000103	-24.40349	-22.53321	9.8	-23.78009	-22.53321	30871.94
9.9	-0.000106	-9.35E-05	-23.25056	-20.51112	9.9	-22.33746	-20.51112	30873.68
10.1	-9.63E-05	-8.53E-05	-21.14294	-18.7137	10.1	-20.33323	-18.7137	30875.58
10.2	-9.19E-05	-8.15E-05	-20.18049	-17.8889	10.2	-19.41667	-17.8889	30876.45
10.3	-8.78E-05	-7.8E-05	-19.27317	-17.1128	10.3	-18.55308	-17.1128	30877.27
10.6	-7.68E-05	-6.85E-05	-16.84621	-15.02519	10.6	-16.23923	-15.02519	30879.47
11	-6.46E-05	-5.8E-05	-14.18441	-12.72261	11	-13.69716	-12.72261	30881.89
13	-3.03E-05	-2.79E-05	-6.65946	-6.113761	13	-6.477563	-6.113761	30888.8
15	-1.62E-05	-1.52E-05	-3.556331	-3.337808	15	-3.48349	-3.337808	30891.69
17	-9.48E-06	-9.02E-06	-2.080157	-1.980562	17	-2.046959	-1.980562	30893.09
20	-4.79E-06	-4.62E-06	-1.051391	-1.014397	20	-1.039059	-1.014397	30894.07
25	-1.92E-06	-1.87E-06	-0.421503	-0.411398	25	-0.418135	-0.411398	30894.69
30	-9.3E-07	-9.13E-07	-0.204094	-0.200303	30	-0.20283	-0.200303	30894.9
40	-3.15E-07	-3.12E-07	-0.069182	-0.068469	40	-0.068944	-0.068469	30895.03

R (Bohr)	SIGMA (Ha	PI (Hartree	SIGMA (cm	PI (cm-1)	R (Bohr)	X (cm-1)	V1 (cm-1)	V2 (cm-1)
1.9	0.99675		218761.2	0				
2	0.804579	0.998666	176584.8	219181.8	2	179568.1	219181.8	226735.5
2.1	0.652882	0.91379	143291	200553.8	2.1	146400	200553.8	207981.8
2.2	0.532183	0.755944	116800.7	165910.6	2.2	119848.3	165910.6	173400.1
2.3	0.435403	0.663809	95560.02	145689.3	2.3	98616.27	145689.3	153170
2.4	0.357231	0.567218	78403.05	124489.9	2.4	81422.83	124489.9	132007.1
2.5	0.293662	0.484993	64451.4	106443.7	2.5	67427.84	106443.7	114004.2
2.6	0.241669	0.414581	53040.32	90989.98	2.6	55965.88	90989.98	98601.42
2.7	0.198946	0.354039	43663.6	77702.48	2.7	46530	77702.48	85373.09
2.8	0.16372	0.301868	35932.31	66252.33	2.8	38730.45	66252.33	73991.2
2.9	0.13461	0.256884	29543.51	56379.42	2.9	32263.53	56379.42	64196.41
3	0.110526	0.218119	24257.64	47871.52	3	26889.03	47871.52	55777.15
3.1	0.09059	0.184761	19882.25	40550.24	3.1	22413.98	40550.24	48555.53
3.2	0.07409	0.15611	16260.86	34262.22	3.2	18681.72	34262.22	42378.37
3.3	0.060439	0.131558	13264.82	28873.74	3.3	15563.81	28873.74	37111.76
3.4	0.049155	0.11057	10788.17	24267.37	3.4	12954.98	24267.37	32637.57
3.5	0.039836	0.092675	8742.893	20339.72	3.5	10768.53	20339.72	28851.09
3.6	0.03215	0.077456	7056.107	16999.6	3.6	8933.474	16999.6	25659.25
3.7	0.025821	0.064548	5667.063	14166.73	3.7	7391.488	14166.73	22979.31
3.8	0.020619	0.05363	4525.301	11770.45	3.8	6094.912	11770.45	20737.85
3.9	0.016351	0.044419	3588.689	9748.929	3.9	5004.587	9748.929	18870.04
4	0.012859	0.03667	2822.237	8048.078	4	4088.381	8048.078	17318.94
4.1	0.010009	0.030167	2196.744	6620.83	4.1	3319.641	6620.83	16034.94
4.2	0.007691	0.024724	1687.935	5426.372	4.2	2676.151	5426.372	14975.17
4.3	0.005812	0.020182	1275.567	4429.426	4.3	2139.149	4429.426	14102.85
4.4	0.004296	0.016401	942.8367	3599.612	4.4	1692.721	3599.612	13386.74
4.5	0.003079	0.013263	675.7141	2910.855	4.5	1323.201	2910.855	12800.38
4.6	0.002108	0.010666	462.5603	2340.833	4.6	1018.858	2340.833	12321.55
4.7	0.001338	0.008523	293.6746	1870.523	4.7	769.5673	1870.523	11931.64
4.8	0.000734	0.00676	161.0044	1483.695	4.8	566.5999	1483.695	11615.11
4.9	0.000264	0.005316	57.86449	1166.639	4.9	402.4647	1166.639	11359.05
5	-9.7E-05	0.004136	-21.29089	907.6746	5	270.7127	907.6746	11152.68
5.1	-0.000369	0.003176	-81.04759	697.0075	5.1	165.8581	697.0075	10987.11
5.2	-0.00057	0.002398	-125.1927	526.3287	5.2	83.21686	526.3287	10854.93
5.3	-0.000715	0.001771	-156.8585	388.7005	5.3	18.82752	388.7005	10750.02
5.4	-0.000814	0.001268	-178.5975	278.2851	5.4	-30.64112	278.2851	10667.34
5.5	-0.000877	0.000867	-192.5319	190.2296	5.5	-67.99667	190.2296	10602.7
5.6	-0.000913	0.000549	-200.3386	120.4718	5.6	-95.55011	120.4718	10552.69
5.7	-0.000927	0.000299	-203.4201	65.65024	5.7	-115.2437	65.65024	10514.48
5.8	-0.000925	0.000105	-202.9065	22.9746	5.8	-128.6811	22.9746	10485.76
5.9	-0.00091	-4.49E-05	-199.6978	-9.864025	5.9	-137.1753	-9.864025	10464.62
6	-0.000886	-0.000158	-194.5226	-34.75161	6	-141.8012	-34.75161	10449.54
6.1	-0.000856	-0.000243	-187.9537	-53.26328	6.1	-143.4378	-53.26328	10439.23
6.2	-0.000822	-0.000304	-180.4411	-66.66761	6.2	-142.7886	-66.66761	10432.69
6.3	-0.000785	-0.000346	-172.3425	-76.02079	6.3	-140.4303	-76.02079	10429.08
6.4	-0.000747	-0.000374	-163.9322	-82.1713	6.4	-136.8192	-82.1713	10427.73
6.5	-0.000708	-0.000391	-155.421	-85.81822	6.5	-132.322	-85.81822	10428.09
6.6	-0.00067	-0.000399	-146.9646	-87.52209	6.6	-127.2248	-87.52209	10429.75
6.7	-0.000632	-0.0004	-138.6794	-87.73975	6.7	-121.7542	-87.73975	10432.34
6.8	-0.000595	-0.000396	-130.6511	-86.83514	6.8	-116.0862	-86.83514	10435.61
6.9	-0.00056	-0.000388	-122.9387	-85.09981	6.9	-110.3559	-85.09981	10439.33

7	-0.000527	-0.000377	-115.5753	-82.76608	7	-104.6616	-82.76608	10443.33
7.1	-0.000495	-0.000365	-108.5873	-80.01674	7.1	-99.08096	-80.01674	10447.49
7.2	-0.000465	-0.000351	-101.9811	-76.99389	7.2	-93.66518	-76.99389	10451.7
7.3	-0.000436	-0.000336	-95.75678	-73.80932	7.3	-88.45111	-73.80932	10455.9
7.4	-0.00041	-0.000321	-89.91217	-70.54793	7.4	-83.46533	-70.54793	10460.02
7.5	-0.000385	-0.000307	-84.43408	-67.27556	7.5	-78.72078	-67.27556	10464.02
7.6	-0.000361	-0.000292	-79.30935	-64.03611	7.6	-74.22319	-64.03611	10467.89
7.7	-0.00034	-0.000277	-74.51822	-60.86632	7.7	-69.97152	-60.86632	10471.6
7.8	-0.000319	-0.000263	-70.04972	-57.79206	7.8	-65.967	-57.79206	10475.14
7.9	-0.0003	-0.00025	-65.8797	-54.83135	7.9	-62.19949	-54.83135	10478.5
8	-0.000282	-0.000237	-61.9928	-51.99354	8	-58.66182	-51.99354	10481.69
8.1	-0.000266	-0.000225	-58.36928	-49.28522	8.1	-55.343	-49.28522	10484.7
8.2	-0.000251	-0.000213	-54.99376	-46.70859	8.2	-52.23348	-46.70859	10487.54
8.3	-0.000236	-0.000202	-51.84869	-44.26803	8.3	-49.32301	-44.26803	10490.22
8.5	-0.00021	-0.000181	-46.18185	-39.77758	8.5	-44.04796	-39.77758	10495.1
8.6	-0.000199	-0.000172	-43.63375	-37.7211	8.6	-41.66361	-37.7211	10497.32
8.7	-0.000188	-0.000163	-41.25465	-35.78534	8.7	-39.43217	-35.78534	10499.4
8.9	-0.000168		-36.9625	0	8.9	-24.67045	0	10524.72
9	-0.00016	-0.00014	-35.02376	-30.63646	9	-33.56173	-30.63646	10504.91
9.1	-0.000151	-0.000133	-33.21324	-29.11989	9.1	-31.84914	-29.11989	10506.53
9.3	-0.000136	-0.00012	-29.93007	-26.3589	9.3	-28.73995	-26.3589	10509.46
9.4	-0.00013	-0.000114	-28.44178	-25.09994	9.4	-27.32807	-25.09994	10510.8
9.7	-0.000112		-24.50737	0	9.7	-16.3509	0	10528.85
9.8	-0.000106	-9.46E-05	-23.35099	-20.7647	9.8	-22.48903	-20.7647	10515.38
9.9	-0.000101	-9.04E-05	-22.26387	-19.83246	9.9	-21.45353	-19.83246	10516.37
10.1	-9.24E-05	-8.26E-05	-20.27583	-18.12317	10.1	-19.55837	-18.12317	10518.17
10.2	-8.82E-05	-7.9E-05	-19.36693	-17.33908	10.2	-18.69107	-17.33908	10519
10.3	-8.43E-05	-7.56E-05	-18.5094	-16.59691	10.3	-17.87198	-16.59691	10519.78
10.6	-7.39E-05	-6.65E-05	-16.2118	-14.60033	10.6	-15.6747	-14.60033	10521.87
11	-6.23E-05	-5.64E-05	-13.68413	-12.38556	11	-13.25131	-12.38556	10524.19
13	-2.95E-05	-2.73E-05	-6.484545	-5.982144	13	-6.317083	-5.982144	10530.86
15	-1.59E-05	-1.49E-05	-3.48376	-3.279535	15	-3.415686	-3.279535	10533.66
17	-9.32E-06	-8.89E-06	-2.045469	-1.951725	17	-2.014221	-1.951725	10535.03
20	-4.73E-06	-4.58E-06	-1.037196	-1.004546	20	-1.026313	-1.004546	10535.99
25	-1.9E-06	-1.86E-06	-0.416213	-0.407331	25	-0.413252	-0.407331	10536.6
30	-9.15E-07	-8.99E-07	-0.200726	-0.197343	30	-0.199598	-0.197343	10536.81
40	-3.04E-07	-3.01E-07	-0.066779	-0.066163	40	-0.066574	-0.066163	10536.94